Third-order transport coefficient tensor of charged-particle swarms in electric and magnetic fields

I. Simonović [1], D. Bošnjaković [1], Z. Lj. Petrović [2], P. Stokes [3], R. D. White,[3] and S. Dujko [1,*]

[1]*Institute of Physics, University of Belgrade, PO Box 68, 11080 Belgrade, Serbia*
[2]*Serbian Academy of Sciences and Arts, Knez Mihailova 35, 11001 Belgrade, Serbia*
[3]*College of Science and Engineering, James Cook University, 4810 Townsville, Australia*

Third-order transport coefficient tensor of charged-particle swarms in neutral gases in the presence of spatially uniform electric and magnetic fields is considered using a multiterm solution of Boltzmann's equation and Monte Carlo simulation technique. The structure of the third-order transport coefficient tensor and symmetries along its individual components in varying configurations of electric and magnetic fields are addressed using a group projector technique and through symmetry considerations of the Boltzmann equation. In addition, we focus upon the physical interpretation of the third-order transport coefficient tensor by considering the extended diffusion equation which incorporates the contribution of the third-order transport coefficients to the density profile of charged particles. Numerical calculations are carried out for electron and ion swarms for a range of model gases with the aim of establishing accurate benchmarks for third-order transport coefficients. The effects of ion to neutral-particle mass ratio are also examined. The errors of the two-term approximation for solving the Boltzmann equation and limitations of previous treatments of the high-order charged-particle transport properties are also highlighted.

I. INTRODUCTION

Studies of charged-particle swarms in neutral gases under the influence of electric and magnetic fields have applications in diverse areas of science and technology ranging from swarm experiments used to determine electron- and ion-neutral cross sections [1–5] to plasma processing technology [6–9], particle detectors used in high-energy physics [10,11], high-voltage technology [12], and positron physics [13,14]. These applications often require knowledge of swarm transport coefficients in the presence of the reduced electric and magnetic fields, E/n_0 and B/n_0, where E and B are the strengths of electric and magnetic fields, respectively, while n_0 is the neutral number density.

There is a large and growing literature dealing with the low-order transport coefficients, in which the variation of the reaction rate, drift velocity and diffusion tensor with E/n_0 (and B/n_0) for both the electrons and ions [15,16], and since recently even for positrons [14,17], are reported. In contrast, little is known about high-order transport coefficients, and limited data can be found in the literature, particularly for light charged particles such as electrons or positrons. The most obvious reason for this situation is the fact that the transport coefficients of higher-order have been difficult to measure, difficult to treat theoretically, and even more difficult to include in plasma models and thus were systematically ignored in the traditional interpretation of swarm experiments [1,3,4,16]. It was usually anticipated that swarm experiments are performed under conditions in which the effects induced by transport coefficients of higher-order are negligible [18,19]. On the other hand, in the early 1970s, it was shown that some arrival-time spectra of ions in drift tubes significantly deviate from the ideal Gaussian pulses which are represented in terms of the lower-order transport coefficients only [20]. To our knowledge, there have been only a few attempts to measure the third-order transport coefficients, or to be more accurate to interpret the observed data in terms of the effects of higher order transport [21–24].

In spite of low interest in higher-order transport coefficients, it was pointed out by several specialists and research groups that the third-order transport coefficients for electrons are very sensitive to the rapid variations with the energy of the momentum transfer cross section as a function of the energy. For example, it was pointed out by Penetrante and Bardsley [18] almost 25 years ago that the third-order transport coefficients are at least as sensitive to the depth and position of the Ramsauer-Townsend minimum for elastic scattering of the electrons in noble gases as the lower-order transport coefficients, including the drift velocity and the characteristic energy. Along similar lines, it was pointed out by Vrhovac *et al.* [19] that the third-order transport coefficients would be very useful for a fine tuning of cross sections for inelastic collisions in the close vicinity of their thresholds. This implies that in principle one could use the higher-order transport coefficients as an additional input for enhancing the reliability of swarm-derived cross sections.

Early work on the higher-order transport coefficients of charged-particle swarms in electric fields has been presented by Whealton and Mason [25]. Using the analytical solution of Boltzmann's equation for the Maxwell model of interaction, they found that the third-order transport coefficient

tensor has seven nonzero elements of which three are independent. It was also shown that when the electric field is absent, all components of the third-order transport coefficient tensor vanish. Early studies of the third-order transport coefficients for ion swarms have been performed by Robson [26] and Larsen *et al.* [27] using Boltzmann's equation solutions.

In 1994, Penetrante and Bardsley [18] carried out the numerical solution of Boltzmann's equation for electrons in noble gases. Among many important points, they found that the third-order transport coefficients could be detected and resolved from the arrival time spectra of an electron swarm. A similar procedure for the determination of the transport coefficients of both the low and higher order was earlier proposed by Kondo and Tagashira [28]. Koutselos used molecular dynamics simulations and a three-temperature treatment of Boltzmann's equation with the aim of calculating the third-order transport coefficients for K^+ and Li^+ ions in noble gases [29–32].

Within the framework of the semiquantitative momentum transfer theory [2,33,34], Vrhovac *et al.* [19] have developed the method of calculations of the third-order transport coefficients for charged-particle swarms in the presence of an electric field only. The theory and the associated numerical code, were used to evaluate the third-order transport coefficients in noble gases, but only in the limit of the lower values of E/n_0 where electrons undergo elastic collisions only. The presented results were found to confirm the structure of the third-order transport coefficient tensor previously determined by Whealton and Mason [25].

Using the theory of arrival time spectra of an electron swarm initially developed by Kondo and Tagashira [28] and a Monte Carlo simulation technique, Kawaguchi and coworkers derived the relation between the longitudinal third-order transport coefficient and the α parameters (arrival-time spectra transport coefficients) [35,36]. Arrival-time spectra can be measured by a double-shutter drift tube clearly indicating that the longitudinal third-order transport coefficient can be obtained experimentally from the knowledge of the α parameters. Along similar lines, it was pointed out by Dujko *et al.* [37] that the conversion of hydrodynamic transport coefficients to those found in the steady-state Townsend experiment requires the knowledge of the third-order transport coefficients. Petrović and co-workers [38] have also used a Monte Carlo simulation technique to derive the longitudinal and transverse third-order transport coefficients in CH_4 over a broad range of the applied reduced electric fields. Among many important points, it was shown that the transverse third-order transport coefficient becomes negative in the same range of the applied electric fields where the negative differential conductivity occurs. The negativity of the third-order transport coefficients has also been observed for charged-particle transport in the presence of trapped (localized) states [39].

The signatures of the higher order transport processes have been observed in the numerical modeling of plasma discharges. For example, in the avalanche phase of the streamer development, the particle-in-cell Monte Carlo simulations have shown that a spatial profile of electrons may significantly deviate from an ideal Gaussian as predicted by fluid models based on the equation of continuity [40,41]. The clear signs

of high-order transport have been observed in the studies of the spatiotemporal development of the electron swarms [42,43]. The pronounced asymmetry in the spatial profiles of the electron swarm is particularly evident during the transient phase of relaxation, in the presence of strong nonconservative interactions [44,45], as well as for electron transport in noble gases with a Ramsauer-Townsend minimum under the influence of E/n_0's for which the mean electron energies are well below the first inelastic threshold. It is worth noting that a similar effect of nonconservative collisions is observed for positrons in gases where spatially dependent positronium formation skews the profile of the ensemble to the point that a Gaussian cannot be recognized and analyzed [46,47].

Furthermore, the transport coefficients of the third and higher orders are very often used to characterize fractional transport in a variety of situations, ranging from the trapping of charge carriers in local imperfections in semiconductors [48–51] to electron [52–54] and positronium [13,55,56] trapping in bubble states within liquids, and to transport in biological cells [57–60].

The above examples clearly show that a rigorous analysis of the third-order transport coefficients in the context of the contemporary kinetic theory of charged-particle swarms is a long overdue, and the present paper takes a few important steps in this direction. Besides being of intrinsic interest, we are also motivated by the following questions: What is the structure of the third-order transport coefficient tensor, and how can symmetries be identified in varying configurations of electric and magnetic fields? What is the physical interpretation of third-order transport coefficients, and what is their contribution to the spatial profile of the swarm in a typical time-of-flight experiment? Is this contribution more significant for light charged particles or for more massive ions? How does the magnetic field affect the third-order transport coefficients, and how large are the errors of the two-term approximation for solving the Boltzmann equation? In the present paper, we will try to address these issues.

This paper is organized as follows. In Sec. II we discuss the basic elements of the theory, the structure and physical interpretation of the third-order transport coefficient tensor, as well as our methods of calculations. In Sec. III we present results of calculations for a range of model gases. Where possible, the results of the Boltzmann equation analysis are compared with those calculated by the Monte Carlo method with the goal of establishing accurate benchmarks for third-order transport coefficients. As an example of our calculations in real gases, in Sec. III we discuss the behavior of the third-order transport coefficients for electron swarms in neon. Last, in Sec. IV we present our conclusions and future work recommendations.

II. THEORY: DEFINITIONS, SYMMETRIES, INTERPRETATIONS, AND METHODS OF CALCULATION

The main physical object of our study is a swarm of charged particles which moves through a background of neutral molecules in external electric and magnetic fields crossed at arbitrary angles. The density of charged particles is assumed to be sufficiently low so that the following properties apply: (1) charged-particle–charged-particle inter-

actions and space charge effects can be neglected, collisions of transported charged particles and excited or dissociated species are unlikely, (2) the motion of charged particles between collisions can be treated classically, and (3) the presence of charged particles does not perturb the background particles from thermal equilibrium.

All information on the drift, diffusion, and transport properties of higher order of charged particles is contained in the charged-particle phase-space distribution function $f(\boldsymbol{r}, \boldsymbol{c}, t)$, where $\boldsymbol{r}$ represents the spatial coordinate of a charged particle at time t, and $\boldsymbol{c}$ denotes its velocity. In the present work, the distribution function $f(\boldsymbol{r}, \boldsymbol{c}, t)$ is determined by solving Boltzmann's equation:

$$\frac{\partial f}{\partial t} + \boldsymbol{c} \cdot \frac{\partial f}{\partial \boldsymbol{r}} + \frac{q}{m}(\boldsymbol{E} + \boldsymbol{c} \times \boldsymbol{B}) \cdot \frac{\partial f}{\partial \boldsymbol{c}} = -J(f, f_0), \quad (1)$$

where q and m are the charge and mass of charged particles, respectively, while the electric and magnetic fields are assumed to be spatially homogeneous and of magnitudes E and B. In the present work we employ a coordinate system in which the z axis is defined by $\boldsymbol{E}$ while $\boldsymbol{B}$ lies in the y-z plane, making an angle ψ with respect to $\boldsymbol{E}$. The right-hand side of (1) denotes the linear charged-particle–neutral-particle collision operator, accounting for elastic and various types of inelastic collisions, including nonconservative collisions (the charged-particle number changing processes, such as ionization and attachment for electron swarms or positronium (Ps) formation and annihilation for positron swarms). The velocity distribution function of the background particles is denoted by f_0, and in the present study it is taken to be a stationary Maxwellian at fixed temperature. The explicit form of the collision operator can be found in Refs. [61,62].

A. Definition of the third-order transport coefficient tensor

The continuity of charged particles in the configuration space requires the following balance equation:

$$\frac{\partial n(\boldsymbol{r}, t)}{\partial t} + \boldsymbol{\nabla} \cdot \boldsymbol{\Gamma}(\boldsymbol{r}, t) = S(\boldsymbol{r}, t), \quad (2)$$

where

$$n(\boldsymbol{r}, t) = \int f(\boldsymbol{r}, \boldsymbol{c}, t) \, d\boldsymbol{c} \quad (3)$$

is the number density of charged particles while $\boldsymbol{\Gamma}(\boldsymbol{r}, t) = n\langle \boldsymbol{c} \rangle$ is the charged-particle flux given by

$$\Gamma(\mathbf{r}, t) = \int \mathbf{c} f(\mathbf{r}, \mathbf{c}, t) \, d\mathbf{c}. \quad (4)$$

The quantity $S(\boldsymbol{r}, t)$ is the production rate per unit volume per unit time arising from nonconservative processes. If the electron-impact ionization and electron attachment are the only nonconservative processes, then this property for electron swarms is given as

$$S(\mathbf{r}, t) = \int n_0 c[\sigma_i(\epsilon) - \sigma_a(\epsilon)] f(\mathbf{r}, \mathbf{c}, t) \, d\mathbf{c}, \quad (5)$$

where $\sigma_i(\epsilon)$ is the cross section for electron impact ionization while σ_a is the cross section for electron attachment. The equation of continuity (2) provides a direct link between experiment and theory, as in the majority of swarm experiments

the experimentally measurable quantities are usually charged-particle currents or charged-particle densities.

In the present work we follow the conventional definitions of transport coefficients and assume that the hydrodynamic conditions prevail, so that all space-time dependence is expressible through linear functionals of $n(\boldsymbol{r}, t)$. The hydrodynamic conditions are not satisfied near the boundaries of the system or in the vicinity of sources and/or sinks of charged particles, as well as under conditions in which electric and/or magnetic fields are not spatially homogeneous. The functional representation of the hydrodynamic approximation is the well-known density gradient expansion of the phase-space distribution function [63]:

$$f(\boldsymbol{r}, \boldsymbol{c}, t) = \sum_{k=0}^{\infty} \boldsymbol{f}^{(k)}(\boldsymbol{c}, t) \odot (-\nabla)^k n(\boldsymbol{r}, t), \quad (6)$$

where $\boldsymbol{f}^{(k)}(\boldsymbol{c}, t)$ are time-dependent tensors of rank k and $\odot$ denotes a k-fold scalar product. Performing equivalent representation of the flux $\boldsymbol{\Gamma}(\boldsymbol{r}, t)$ and source term $S(\boldsymbol{r}, t)$, we have

$$\boldsymbol{\Gamma}(\boldsymbol{r}, t) = \sum_{k=0}^{\infty} \boldsymbol{\Gamma}^{(k+1)}(t) \odot (-\nabla)^k n(\boldsymbol{r}, t), \quad (7)$$

$$S(\boldsymbol{r}, t) = \sum_{k=0}^{\infty} \boldsymbol{S}^{(k)}(t) \odot (-\nabla)^k n(\boldsymbol{r}, t), \quad (8)$$

where the superscripts (k) and $(k + 1)$ denote the ranks of the tensors. Equation (7) represents the flux-gradient relation and truncation of the expansion at $k = 2$ gives

$$\boldsymbol{\Gamma}(\boldsymbol{r}, t) = \boldsymbol{W} n(\boldsymbol{r}, t) - \boldsymbol{D} \odot \nabla n(\boldsymbol{r}, t) + \boldsymbol{Q} \odot (\nabla \otimes \nabla) n(\boldsymbol{r}, t), \quad (9)$$

where $\otimes$ is the tensor product, $\boldsymbol{W}$ and $\boldsymbol{D}$ are lower-order transport coefficients, the flux drift velocity and flux diffusion tensor, respectively, and $\boldsymbol{Q}$ defines the flux third-order transport coefficient tensor. The flux transport coefficients are given by

$$\mathbf{W} = \boldsymbol{\Gamma}^{(1)} = \int \mathbf{c} \boldsymbol{f}^{(1)}(\mathbf{c}, t) \, d\mathbf{c}, \quad (10)$$

$$\mathbf{D} = \boldsymbol{\Gamma}^{(2)} = \int \mathbf{c} \boldsymbol{f}^{(2)}(\mathbf{c}, t) \, d\mathbf{c}, \quad (11)$$

$$\mathbf{Q} = \boldsymbol{\Gamma}^{(3)} = \int \mathbf{c} \boldsymbol{f}^{(3)}(\mathbf{c}, t) \, d\mathbf{c}, \quad (12)$$

where $\boldsymbol{f}^{(1)}(\mathbf{c}, t)$, $\boldsymbol{f}^{(2)}(\mathbf{c}, t)$, and $\boldsymbol{f}^{(3)}(\mathbf{c}, t)$ are the expansion coefficients in the density-gradient expansion of the phase-space distribution function (6).

Substitution of expansions (7) and (8) into the continuity equation (2) yields the extended diffusion equation which incorporates the contribution of the third-order transport coefficient tensor,

$$\frac{\partial n(\boldsymbol{r}, t)}{\partial t} + \boldsymbol{W}^{(b)} \odot \nabla n(\boldsymbol{r}, t) - \boldsymbol{D}^{(b)} \odot (\nabla \otimes \nabla) n(\boldsymbol{r}, t)$$
$$+ \boldsymbol{Q}^{(b)} \odot (\nabla \otimes \nabla \otimes \nabla) n(\boldsymbol{r}, t) = -R_{\text{net}} n(\boldsymbol{r}, t), \quad (13)$$

where R_{net} is the net particle loss rate. For electron swarms, this quantity is given by

$$R_{net} = -S^{(0)} = -\iint n_0 c[\sigma_i(\epsilon) - \sigma_a(\epsilon)]f(\mathbf{r}, \mathbf{c}, t)\, d\mathbf{c}\, d\mathbf{r}.$$
(14)

$\mathbf{W}^{(b)}$ and $\mathbf{D}^{(b)}$ are the bulk drift velocity and bulk diffusion tensor, respectively, and $\mathbf{Q}^{(b)}$ is the bulk third-order transport coefficient tensor. The connection between the bulk and flux transport coefficients is given by

$$\mathbf{W}^{(b)} = \mathbf{W} + \mathbf{S}^{(1)}, \quad \mathbf{D}^{(b)} = \mathbf{D} + \mathbf{S}^{(2)}, \quad \mathbf{Q}^{(b)} = \mathbf{Q} + \mathbf{S}^{(3)},$$
(15)

where $\mathbf{S}^{(1)}$, $\mathbf{S}^{(2)}$, and $\mathbf{S}^{(3)}$ are the expansion coefficients in the hydrodynamic expansion of the source term (8).

The third-order transport coefficient tensor is referred to as the *skewness coefficient* by some authors [18], while other authors use the term *skewness* to denote just the diagonal component of this tensor along the direction of the electric field [19]. For brevity, in the rest of this work we will sometimes refer to the third-order transport coefficient tensor as the skewness tensor.

In the absence of nonconservative processes (or when the collision frequencies of these processes are independent of the energy) the bulk and the flux transport coefficients are equal [64]. In the presence of nonconservative collisions these two families of transport coefficients can vary quite substantially from each other. The physical interpretation, the origin of differences and the application of the bulk and flux low-order transport coefficients as well as their application in the modeling of plasma discharges have been thoroughly discussed and illustrated in our previous publications [6,16,41,62]. We defer a full discussion of the differences between the bulk and flux third-order tensor coefficients to a future publication.

In order to show the rank of the tensor explicitly, the third-order transport coefficient tensor in (9) can be rewritten

$$[\mathbf{Q} \odot (\nabla \otimes \nabla)n]_i \equiv \sum_{jk} Q_{ijk} \frac{\partial^2 n(\mathbf{r}, t)}{\partial x_j \partial x_k},$$
(16)

where the indices i, j, k each run over the space coordinates x, y, z. We note that there are 27 components in the tensor $\mathbf{Q}$ without considering any symmetry of the system under permutation operations. However, since the order of differentiation of n is irrelevant, some components of a tensor must be equal to each other. For example, for the magnetic-field-free case the maximal number of independent components is three, while when both the electric and magnetic fields are present and crossed at an arbitrary angle the maximal number of independent components is 18. It is clear that the structure of a tensor and symmetries along individual components depend on the field configuration.

B. Structure and symmetry considerations of the third-order transport coefficient tensor

One of the most important tasks in analysis of higher-order transport coefficients is to identify the symmetries along individual elements of the tensors. In this section we apply the group projector method [65] to determine the structure

of the skewness tensor. The group projector method is briefly discussed in Appendix A.

We first consider a magnetic-field-free case. The symmetry group of the system in the magnetic-field-free configuration is $C_{\infty V}$ (see Appendix A). This group has two connected components. The first component corresponds to rotations $R_z(\alpha)$ about the z axis through an arbitrary angle α. The second component corresponds to the composition of a rotation $R_z(\alpha)$ and a reflection in the symmetry plane σ_v. Polar vector (PV) representations of the group elements from the first and the second connected components are

$$D^{PV}(R_z(\alpha)) = \begin{pmatrix} \cos\alpha & -\sin\alpha & 0 \\ \sin\alpha & \cos\alpha & 0 \\ 0 & 0 & 1 \end{pmatrix},$$
(17)

$$D^{PV}(\sigma_v R_z(\alpha)) = \begin{pmatrix} \cos\alpha & -\sin\alpha & 0 \\ -\sin\alpha & -\cos\alpha & 0 \\ 0 & 0 & 1 \end{pmatrix},$$
(18)

where α is the angle of rotation around the z axis. Thus, for the magnetic-field-free case the following structure of the skewness tensor is derived:

$$Q_{xab} = \begin{pmatrix} 0 & 0 & Q_{xxz} \\ 0 & 0 & 0 \\ Q_{xxz} & 0 & 0 \end{pmatrix}, \quad Q_{yab} = \begin{pmatrix} 0 & 0 & 0 \\ 0 & 0 & Q_{xxz} \\ 0 & Q_{xxz} & 0 \end{pmatrix},$$

$$Q_{zab} = \begin{pmatrix} Q_{zxx} & 0 & 0 \\ 0 & Q_{zxx} & 0 \\ 0 & 0 & Q_{zzz} \end{pmatrix},$$
(19)

where $a, b \in \{x, y, z\}$. For the magnetic-field-free case the skewness tensor has seven nonzero elements and only three independent elements, including Q_{zzz}, Q_{zxx}, and Q_{xxz} [19,25,31,32]. Furthermore, the following symmetry properties along the individual elements of the tensor hold:

$$Q_{xxz} = Q_{xzx} = Q_{yyz} = Q_{yzy}, \quad Q_{zxx} = Q_{zyy}.$$
(20)

For parallel electric and magnetic fields the symmetry group of the system is C_∞ (see Appendix A). This group has only a single component consisting of rotations $R_z(\alpha)$:

$$D^{PV}(R_z(\alpha)) = \begin{pmatrix} \cos\alpha & -\sin\alpha & 0 \\ \sin\alpha & \cos\alpha & 0 \\ 0 & 0 & 1 \end{pmatrix}.$$
(21)

In this case the structure of the skewness tensor is more complicated. For instance, the presence of the element Q_{xyz} is due to the explicit effects of the magnetic field on the trajectories of the charged particles. It is interesting to note that this component has exactly the opposite contribution to the third-order diffusive flux along the x and y directions. This is analogous to the D_{xy} component of the diffusion tensor. Likewise, the third-order flux along the magnetic field direction is the same as for the magnetic-field-free case. Thus, for parallel electric and magnetic fields the skewness tensor

has the following structure:

$$Q_{xab} = \begin{pmatrix} 0 & 0 & Q_{xxz} \\ 0 & 0 & Q_{xyz} \\ Q_{xxz} & Q_{xyz} & 0 \end{pmatrix},$$

$$Q_{yab} = \begin{pmatrix} 0 & 0 & -Q_{xyz} \\ 0 & 0 & Q_{xxz} \\ -Q_{xyz} & Q_{xxz} & 0 \end{pmatrix}, \qquad (22)$$

$$Q_{zab} = \begin{pmatrix} Q_{zxx} & 0 & 0 \\ 0 & Q_{zxx} & 0 \\ 0 & 0 & Q_{zzz} \end{pmatrix}.$$

For parallel electric and magnetic fields the skewness tensor has 11 nonzero elements and only four independent elements, including Q_{zzz}, Q_{zxx}, Q_{xxz}, and Q_{xyz}. Furthermore, the following symmetry properties along the individual elements of the tensor may be identified:

$$Q_{xxz} = Q_{xzx} = Q_{yyz} = Q_{yzy}, \quad Q_{zxx} = Q_{zyy},$$

$$Q_{xyz} = Q_{xzy} = -Q_{yxz} = -Q_{yzx}. \qquad (23)$$

For orthogonal electric and magnetic fields the symmetry group of the system is C_{1V}. This group has only two elements, the unity element e and a reflection in the symmetry plane σ_v, which is orthogonal to the direction of the magnetic field. The PV representations of these two elements are given by

$$D^{PV}(e) = \begin{pmatrix} 1 & 0 & 0 \\ 0 & 1 & 0 \\ 0 & 0 & 1 \end{pmatrix}, \quad D^{PV}(\sigma_v) = \begin{pmatrix} 1 & 0 & 0 \\ 0 & -1 & 0 \\ 0 & 0 & 1 \end{pmatrix}. \quad (24)$$

Thus, for orthogonal electric and magnetic fields the skewness tensor has the following structure:

$$Q_{xab} = \begin{pmatrix} Q_{xxx} & 0 & Q_{xxz} \\ 0 & Q_{xyy} & 0 \\ Q_{xxz} & 0 & Q_{xzz} \end{pmatrix},$$

$$Q_{yab} = \begin{pmatrix} 0 & Q_{yyx} & 0 \\ Q_{yyx} & 0 & Q_{yyz} \\ 0 & Q_{yyz} & 0 \end{pmatrix}, \qquad (25)$$

$$Q_{zab} = \begin{pmatrix} Q_{zxx} & 0 & Q_{zzx} \\ 0 & Q_{zyy} & 0 \\ Q_{zzx} & 0 & Q_{zzz} \end{pmatrix}.$$

We observe that for orthogonal fields the skewness tensor has 14 nonzero elements among which 10 are independent. The following symmetry properties along the individual elements of the tensor are clearly evident:

$$Q_{xxz} = Q_{xzx}, \quad Q_{yyz} = Q_{yzy}, \quad Q_{yyx} = Q_{yxy}, \quad Q_{zzx} = Q_{zxz}. \qquad (26)$$

When electric and magnetic fields are crossed at arbitrary angles, the symmetry group of the system is the trivial group, which has only the unity element, e.g.,

$$D^{PV}(e) = \begin{pmatrix} 1 & 0 & 0 \\ 0 & 1 & 0 \\ 0 & 0 & 1 \end{pmatrix}. \qquad (27)$$

For this general configuration, the skewness tensor is full, and it has 27 nonzero elements. However, there are only 18 independent components as the last two indices of the skewness tensor commute. Thus, the skewness tensor has the following structure:

$$Q_{xab} = \begin{pmatrix} Q_{xxx} & Q_{xxy} & Q_{xxz} \\ Q_{xxy} & Q_{xyy} & Q_{xyz} \\ Q_{xxz} & Q_{xyz} & Q_{xzz} \end{pmatrix},$$

$$Q_{yab} = \begin{pmatrix} Q_{yxx} & Q_{yyx} & Q_{yxz} \\ Q_{yyx} & Q_{yyy} & Q_{yyz} \\ Q_{yxz} & Q_{yyz} & Q_{yzz} \end{pmatrix}, \qquad (28)$$

$$Q_{zab} = \begin{pmatrix} Q_{zxx} & Q_{zxy} & Q_{zzx} \\ Q_{zxy} & Q_{zyy} & Q_{zzy} \\ Q_{zzx} & Q_{zzy} & Q_{zzz} \end{pmatrix}.$$

For this general configuration, one may identify the following symmetry properties along the individual elements:

$$Q_{xxy} = Q_{xyx}, \quad Q_{yyx} = Q_{yxy}, \quad Q_{zzx} = Q_{zxz},$$

$$Q_{xxz} = Q_{xzx}, \quad Q_{yyz} = Q_{yzy}, \quad Q_{zzy} = Q_{zyz}, \qquad (29)$$

$$Q_{xyz} = Q_{xzy}, \quad Q_{yzx} = Q_{yxz}, \quad Q_{zxy} = Q_{zyx}.$$

These symmetry arguments can be extended to any of the higher-order transport coefficients.

C. Physical interpretation of the third-order transport coefficients

In this section we discuss the physical meaning of the third-order transport coefficients. Let us assume that the contribution of the third-order transport coefficients to the density profile of charged particles is negligibly small. This reduces the extended diffusion equation (13) to the well-known form

$$\frac{\partial n(\boldsymbol{r}, t)}{\partial t} + \boldsymbol{W}^{(b)} \odot \boldsymbol{\nabla} n(\boldsymbol{r}, t) - \boldsymbol{D}^{(b)} \odot (\boldsymbol{\nabla} \otimes \boldsymbol{\nabla}) n(\boldsymbol{r}, t)$$

$$= -R_{\text{net}} n(\boldsymbol{r}, t). \qquad (30)$$

Swarm experiments are traditionally analyzed by solving the the diffusion equation (30), which gives the density of charged particles throughout the bulk of medium. For example, in an idealized time-of-flight experiment, in which a pulse of N_0 particles is released from a plane source at $z = 0$ at time $t = 0$ into an unbounded medium, the initial and boundary conditions are

$$n(\mathbf{r}, 0) = N_0 \delta(\mathbf{r}),$$

$$n(\mathbf{r}, t) = 0 \ (\|\mathbf{r}\| \to \infty, \ t > 0), \qquad (31)$$

respectively, and the solution is

$$n^{(0)}(\boldsymbol{r}, t) = \frac{N_0 e^{-R_{\text{net}} t} e^{-\frac{\left(z - W^{(b)} t\right)^2}{4 D_L^{(b)} t} - \frac{x^2 + y^2}{4 D_T^{(b)} t}}}{\left(4 \pi D_T^{(b)} t\right) \sqrt{4 \pi D_L^{(b)} t}}, \qquad (32)$$

where $D_L^{(b)}$ and $D_T^{(b)}$ are the bulk longitudinal and bulk transverse diffusion coefficients, respectively, while x, y, and z are the Cartesian coordinates [62]. The solution (32) represents a Gaussian pulse, the peak of which drifts with the velocity $W^{(b)}$ and diffuses about the center of mass according to the diffusion coefficients $D_L^{(b)}$ and $D_T^{(b)}$. For brevity, in what follows

we omit explicit reference to the type of transport coefficients, e.g., the superscripting for all transport coefficients.

Assuming the above initial conditions (31), the extended diffusion equation (13), which incorporates the effects of the third-order transport coefficient tensor, cannot be solved analytically. Thus, we have applied the following procedure. First, the Fourier transform of the charged-particle density is expanded in terms of the longitudinal Q_L and transverse Q_T components of the third-order transport coefficient tensor. Using the inverse Fourier transformation of the expansion coefficients, we have derived the density of charged particles in which the corrections due to the third-order transport coefficients are included. In the first approximation, in which only the first-order corrections are assumed, the density of charged particles is given by

$$n^{(1)}(\boldsymbol{r},t) = \left[1 + Q_L \frac{t(z-Wt)^3 - 6D_L t^2(z-Wt)}{8(D_L t)^3} \right.$$
$$\left. + Q_T \frac{3t(z-Wt)(x^2+y^2-4D_T t)}{8D_L t(D_T t)^2} \right] n^{(0)}(\boldsymbol{r},t). \tag{33}$$

The first-order correction along the longitudinal direction shown in Eq. (33) has been previously published by Penetrante and Bardsley [18]. This equation has a simpler form in relative coordinates that are defined as

$$\chi_z = \frac{z - W^{(b)}t}{\sqrt{2D_L^{(b)}t}}, \quad \chi_x = \frac{x}{\sqrt{2D_T^{(b)}t}}, \quad \chi_y = \frac{y}{\sqrt{2D_T^{(b)}t}}. \tag{34}$$

In these coordinates the approximate solution (32) may be written as

$$n^{(1)}(\boldsymbol{r},t) = n^{(0)}(\boldsymbol{r},t)\left[1 + \frac{tQ_L^{(b)}}{\sigma_z^3}\chi_z(\chi_z^2 - 3) \right.$$
$$\left. + \frac{3tQ_T^{(b)}}{\sigma_x^2\sigma_z}\chi_z(\chi_x^2 + \chi_y^2 - 2) \right]. \tag{35}$$

It can be seen from Eq. (35) that the third-order transport coefficients describe elongation and compression of the number density of charged particles along different parts of the swarm. The detailed physical interpretation of the individual components of the third-order transport tensor is given in Appendix B.

D. Multiterm solutions of Boltzmann's equation

In this section we briefly describe the basic elements of a multiterm theory for solving the Boltzmann equation that has been used to calculate the components of the third-order transport coefficient tensor. The method is by now standard, and for details the reader is referred to our previous publications [66–68]. In brief, the dependence of the phase-space distribution function on the velocity coordinates is represented by its expansion in terms of spherical harmonics (angular dependence) and Sonine polynomials (speed dependence). Likewise, under hydrodynamic conditions a sufficient representation of the space dependence is an expansion in terms of the powers of the density gradient operator. After truncation and discretizing in time, the above expansions allow

a decomposition of the Boltzmann equation into a set of matrix equations in terms of the expansion coefficients which represent the moments of the distribution function. This set of matrix equations can be solved numerically by using the matrix inversion. Transport properties including mean energy, drift velocity, and components of the diffusion tensor can then be calculated directly from the moments of the phase-space distribution function.

In order to find the explicit expressions for the individual elements of the third-order transport coefficient tensor we use the definition of the spherical vector [69]:

$$c_m^{[1]} = \sqrt{\frac{4\pi}{3}} c Y_m^{[1]}(\hat{\boldsymbol{c}}). \tag{36}$$

The connection between Cartesian and spherical components of the velocity vector is given by

$$c_x = \frac{i}{\sqrt{2}}\left(c_1^{[1]} - c_{-1}^{[1]}\right), \quad c_y = \frac{1}{\sqrt{2}}\left(c_1^{[1]} + c_{-1}^{[1]}\right),$$
$$c_z = -ic_0^{[1]}. \tag{37}$$

Likewise, the flux of charged particles in irreducible tensor notation is given by

$$\Gamma_m^{[1]} = n\langle c_m^{[1]}\rangle, \tag{38}$$

while its connection with the Cartesian components is expressed by

$$\Gamma_x = \frac{i}{\sqrt{2}}\left(\Gamma_1^{[1]} - \Gamma_{-1}^{[1]}\right), \Gamma_y = \frac{1}{\sqrt{2}}\left(\Gamma_1^{[1]} + \Gamma_{-1}^{[1]}\right), \tag{39}$$
$$\Gamma_z = -i\Gamma_0^{[1]}.$$

Using the orthogonality relations for spherical harmonics and modified Sonine polynomials [61,69] and relation

$$c^l = \left(\frac{\sqrt{2}}{\alpha}\right)\frac{R_{0l}(\alpha c)}{N_{0l}}, \tag{40}$$

after some algebra we get the following expression for the flux of charged particles in the basis of Sonine polynomials:

$$\Gamma_m^{(1)} = \frac{1}{\alpha}\sum_{s=0}^{\infty}\sum_{\lambda=0}^{s}\sum_{\mu=-\lambda}^{\lambda} F(01m|s\lambda\mu)G_\mu^{(s\lambda)}n(\boldsymbol{r},t). \tag{41}$$

Using the explicit expressions for the irreducible gradient tensor operator in the spherical form of the flux-gradient relation (41) [61], the relationship between the spherical quantities $\Gamma_m^{(1)}$ (where $m = -1, 0, 1$) and their Cartesian counterparts in (9) can be established. The explicit expressions for the individual elements of the flux third-order transport coefficient tensor in the absence of a magnetic field are given by

$$Q_{xxz} = \frac{1}{\sqrt{2}\alpha}[\text{Im}(F(011|221;\alpha)) - \text{Im}(F(01-1|221;\alpha))], \tag{42}$$

$$Q_{zxx} = -\frac{1}{\alpha}\left[\frac{1}{\sqrt{3}}\text{Im}(F(010|200;\alpha)) + \frac{1}{\sqrt{6}}\text{Im}(F(010|220;\alpha))\right]$$
$$+ \frac{1}{\alpha}\text{Im}(F(010|222;\alpha)), \tag{43}$$

$$Q_{zzz} = \frac{1}{\alpha}\left[\sqrt{\frac{2}{3}}\,\mathrm{Im}(F(010|220;\alpha)) - \frac{1}{\sqrt{3}}\mathrm{Im}(F(010|200;\alpha))\right],$$

(44)

where $\mathrm{Re}(\cdot)$ and $\mathrm{Im}(\cdot)$, respectively, represent the real and imaginary parts of the moments. The explicit expressions for the individual elements of the flux skewness tensor in varying configurations of electric and magnetic fields are given in Appendix C. Expressions for the lower-order transport coefficients in terms of the moments of the distribution function can be found in our previous work [66–68,70].

E. Monte Carlo simulation method

The Monte Carlo simulation technique is used in this work as an independent tool to confirm the numerical accuracy and integrity of a multiterm solution of Boltzmann's equation. The Monte Carlo code applied in this work has been systematically tested for a range of model and real gases under both the hydrodynamic and nonhydrodynamic conditions in the presence of the electric and magnetic fields [67,68,71,72]. The subject of testing were the lower-order transport coefficients usually in the presence of nonconservative collisions. In the present work, we follow a large number of particles ($\sim 10^7$) moving in an infinite gas under the influence of spatially homogeneous electric and magnetic fields. Such a large number of charged particles is followed with the aim of reducing the statistical fluctuations of the output data required for the evaluation of the individual elements of the third-order transport coefficient tensor. The charged-particle trajectories between collisions are determined by solving the collisionless equation of motion of a charged particle. The position and velocity of each charged particle are updated after the time step Δt, which is obtained by solving the equation for collision probability. The numerical solution of this equation requires the extensive use of random numbers. The type of collision is also determined using random numbers as well as relative probabilities for individual collisional processes. The details of our Monte Carlo method are given in our several previous publications [67,71–73].

The third-order transport coefficients are determined after relaxation to the steady state. The flux third-order transport coefficient tensor is defined by

$$Q_{abc} = \frac{1}{3!}\left\langle \frac{d}{dt}\left(r_a^* r_b^* r_c^*\right)\right\rangle,$$

(45)

where (a, b, c) take values from the set $\{x, y, z\}$ while the angular brackets $\langle\rangle$ denote ensemble averages in phase space, and $\boldsymbol{r}^* = \boldsymbol{r} - \langle\boldsymbol{r}\rangle$.

It is important to note that although the third-order transport coefficient tensor has the three independent elements when the swarm is acted on solely by the electric field, we are able to identify only two independent elements in our Monte Carlo simulations. This follows from the fact that the expressions for sampling the third-order transport coefficients are derived from the generalized diffusion equation in which all tensor components are contracted with the corresponding partial derivatives of charged-particle density with respect to the coordinates. Thus, the expressions for evaluation the skewness coefficients represent the sum of all skewness tensor

components Q_{abc} which have the same combination of indicies a, b, c where (a, b, c) take values from the set $\{x, y, z\}$. Therefore, the expressions for skewness coefficients in our Monte Carlo simulations are symmetric with respect to the permutation of any two indices. The analogy with the determination of the off-diagonal elements of the diffusion tensor is clearly evident. For example, for perpendicular electric and magnetic fields, we are not able to isolate and evaluate the individual off-diagonal elements of the diffusion tensor [67]. However, it is possible to determine the sum of the individual off-diagonal elements which is the well-known Hall diffusion coefficient. To calculate the individual elements of the third-order transport coefficient tensor and diffusion tensor, one must integrate the velocity over the corresponding hydrodynamic component of the distribution function in velocity space. This is beyond the scope of this work, and we defer this procedure to a future paper.

Due to inability to isolate the individual elements of the third-order transport coefficient tensor in our Monte Carlo simulations, we define the following third-order transport coefficients:

$$Q_{zzz} \equiv Q_L, \quad Q_{\pi(xxz)} \equiv Q_T,$$

(46)

where

$$Q_{\pi(xxz)} = \tfrac{1}{3}(Q_{xxz} + Q_{xzx} + Q_{zxx}),$$

(47)

and $\pi(abc)$ denote all possible permutations of (a, b, c).

The explicit form of the flux longitudinal and flux transverse third-order coefficients are calculated from

$$Q_L = \tfrac{1}{6}(3\langle z^2 c_z\rangle - 3\langle c_z\rangle\langle z^2\rangle - 6\langle z\rangle\langle zc_z\rangle + 6\langle z\rangle\langle z\rangle\langle c_z\rangle), \quad (48)$$

$$Q_T = \tfrac{1}{6}(\langle x^2 c_z\rangle + 2\langle zxc_x\rangle - \langle c_z\rangle\langle x^2\rangle - 2\langle z\rangle\langle xc_x\rangle), \quad (49)$$

where c_x, c_y, and c_z are velocity components. Explicit formulas for the elements of the flux third-order transport coefficient tensor which can be isolated and determined individually in our Monte Carlo simulations in various configurations of the electric and magnetic fields are given in the Appendix C.

III. RESULTS

A. Preliminaries

The aim of the present section is to highlight the general features of the third-order transport coefficients associated with the light charged-particle swarms in gases when both the electric and magnetic fields are present. Benchmark calculations are performed for a range of model gases, including the Maxwell (constant collision frequency) model, the hard-sphere model and the Reid ramp inelastic model. For the present study we consider conservative collisions only. We defer the investigation of the explicit effects of nonconservative collisions on the third-order transport coefficient tensor to a future study. The utility of model gases lies in the fact that through the use of simple analytically given cross sections we can isolate and elucidate physical processes which govern and control the specific behavior of a charged-particle swarm. This is particularly important for higher-order transport coefficients due to complexity of factors which contribute to, or influence, the corresponding tensors. However, the present theory and associated codes have been applied to a number of gases

and mixtures and preliminary results are available elsewhere [74–76]. Here we present some results for neon and compare them with the results of calculations that have been presented elsewhere. We employ the set of cross sections for electron scattering in neon developed by Hayashi [77] (see Fig. 2 in Ref. [78]).

In the Boltzmann equation analysis of the third-order transport coefficients the elastic collisions are treated using the original Boltzmann collision operator [79], while its semiclassical generalization is applied for inelastic processes [80]. All scattering is assumed isotropic and hence for elastic scattering we use the elastic momentum transfer cross section. Calculations are performed assuming that the internal states are governed by a Maxwell-Boltzmann distribution which essentially places all neutral particles in the ground state for systems considered. The thermal motion of background particles is carefully considered in both the Boltzmann equation analysis and Monte Carlo simulations [81].

The Monte Carlo results are presented with error bars. These error bars are required since the third-order transport coefficients are derived from the third-order monomials of coordinates and velocities which usually have high standard deviations. The statistical error of the third-order transport coefficients that are evaluated in our Monte Carlo simulations is estimated as the standard error. The standard error is equal to the standard deviation of the third-order transport coefficients divided by the square root of the number of electrons followed in the simulation. Thus, it is necessary to follow a large number of electrons (at least 10^7) in our Monte Carlo simulations in order to sufficiently reduce the standard error of the final results.

When the magnetic field is applied, the results and discussion are restricted to a crossed field configuration, although the theory and associated codes are valid for arbitrary field configurations. We use the unit of the Townsend (1 Td = 10^{-21} Vm^2) for the reduced electric field and the unit of the Huxley (1 Hx = 10^{-27} Tm^3) for the reduced magnetic field.

B. The Maxwell model

In this section we present benchmark results for the third-order transport coefficients assuming the Maxwell model of interaction. In this model the electrons undergo elastic collisions only and the collision frequency is independent of the energy. The details of the model used here are as follows:

$$\sigma_m(\epsilon) = A\epsilon^{-1/2} \text{ Å}^2 \quad \text{(elastic cross section)},$$

$$m_0 = 4 \text{ amu}, \quad m = 5.486 \times 10^{-4} \text{ amu}, \quad T_0 = 293 \text{ K},$$

$$(50)$$

where ϵ is in eV, m is the electron mass and m_0 is the neutral mass. While the magnitude of potential for elastic scattering A in previous works was usually fixed to a single value of 6 [70,82,83], in the present work its value is varied in order to investigate the influence of elastic collisions on the third-order transport coefficients. We consider the reduced electric field range: 0.1–10 Td.

The results are obtained from the numerical solution of Boltzmann's equation and are presented in Table I. The three

TABLE I. Third-order transport coefficients for the Maxwell model. The results are presented as a function of the reduced electric field E/n_0 and the magnitude of potential for elastic scattering A.

A	E/n_0 (Td)	$n_0^2 Q_{xzx}$ (m^{-3} s^{-1})	$n_0^2 Q_{zxx}$ (m^{-3} s^{-1})	$n_0^2 Q_{zzz}$ (m^{-3} s^{-1})
1.0	0.1	5.2930×10^{45}	2.1761×10^{42}	1.0588×10^{46}
	1.0	4.3919×10^{48}	1.8055×10^{45}	8.7856×10^{48}
	10.0	4.3829×10^{51}	1.8017×10^{48}	8.7676×10^{51}
3.0	0.1	5.1740×10^{43}	2.1279×10^{40}	1.0351×10^{44}
	1.0	1.8373×10^{46}	7.5531×10^{42}	3.6754×10^{46}
	10.0	1.8039×10^{49}	7.4158×10^{45}	3.6087×10^{49}
6.0	0.1	4.7768×10^{42}	1.9648×10^{39}	9.5557×10^{42}
	1.0	6.0575×10^{44}	2.4903×10^{41}	1.2118×10^{45}
	10.0	5.6405×10^{47}	2.3187×10^{44}	1.1283×10^{48}
12.0	0.1	5.4425×10^{41}	2.2388×10^{38}	1.0888×10^{42}
	1.0	2.2880×10^{43}	9.4070×10^{39}	4.5769×10^{43}
	10.0	1.7665×10^{46}	7.2623×10^{42}	3.5340×10^{46}

independent elements of the third-order transport coefficient tensor are given as a function of the reduced electric field E/n_0 and the magnitude of potential for elastic scattering A. We observe that $n_0^2 Q_{xzx}$, $n_0^2 Q_{zxx}$, and $n_0^2 Q_{zzz}$ are positive and monotonically increasing functions of E/n_0. For brevity, in what follows we omit n_0^2, and $n_0^2 Q_{abc}$ will be written as Q_{abc}, where $a, b, c \in \{x, y, z\}$. In the logarithmic plot, the E/n_0 dependence of Q_{xzx}, Q_{zxx}, and Q_{zzz} is linear both for the higher values of E/n_0, where the diffusion deviates significantly from the thermal values, and for the lower values of E/n_0, where the diffusion is essentially thermal. However, the slope of these two linear dependencies is not the same. The slope is greater for those values of E/n_0 for which the diffusion is no longer thermal.

We observe that the Q_{zxx} is less than the remaining elements, Q_{xzx} and Q_{zzz} for all E/n_0 and A considered. The coefficient Q_{zxx} represents the difference in the flux of charged particles along the z direction between the center of the swarm and the transverse edges (see Appendix B). Since the collision frequency for the Maxwell model is independent of energy, the positive value of Q_{zxx} is a clear sign that the mobility of the electrons is greater at the transverse edges than at the center of the swarm, due to a parabolic increase of the mean energy along the transverse direction. This effect is very small and hence the coefficient Q_{zxx} is dominated by the coefficients Q_{xzx} and Q_{zzz}. This physical picture is no more valid for real gases in which the momentum transfer collision frequency is usually a complex function of the electron energy.

Comparing Q_{xzx} and Q_{zzz}, we observe that these two coefficients are of the same order of magnitude for all E/n_0 and A considered. In a certain way this is analogous to the behavior of the diffusion coefficients. For the Maxwell model the longitudinal and transverse diffusion coefficients are equal [82,83]. Likewise, the sum of the coefficients Q_{xzx} and Q_{xxz} which is proportional to the flux along the transverse direction, is equal to the coefficient Q_{zzz} which determines the corresponding flux along the field direction (note that the coefficient Q_{zxx} is negligible as compared to the coefficients Q_{xzx} and Q_{zzz}).
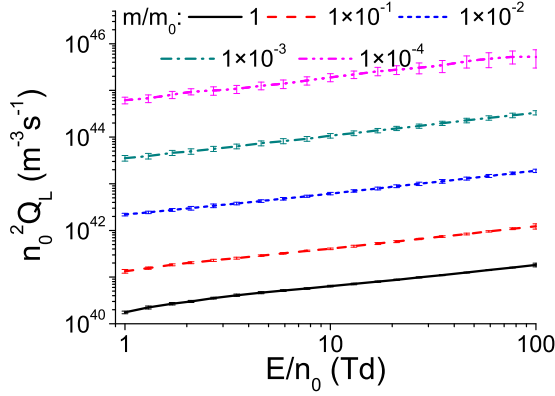
FIG. 1. Influence of the charged-particle to neutral-particle mass ratio on the variation of the longitudinal third-order transport coefficient $n_0^2 Q_L$ with E/n_0 for the hard sphere model. Calculations are performed using a Monte Carlo simulation technique.

C. Effects of the ion to neutral-particle mass ratio

In this section we explore the effects of the ion to neutral mass ratio on the variation of the third-order transport coefficients with E/n_0. Calculations are performed by a Monte Carlo simulation technique assuming the hard sphere model [84]. The details of the model are

$$\sigma_m(\epsilon) = 6 \ \text{Å}^2 \quad \text{(elastic cross section)},$$
$$m_0 = 4 \ \text{amu}, \quad T_0 = 293 \ \text{K}. \tag{51}$$

We consider the mass ratio range 10^{-4}–1 and the reduced electric field range 1–100 Td.

In Fig. 1 we show the variation of the coefficient Q_L as a function of E/n_0 for various charged-particle to neutral-particle mass ratios, as indicated on the graph. For decreasing m/m_0 the energy transfer in elastic collisions is reduced, which in turn increases Q_L. In Monte Carlo simulations, the reduced energy transfer in elastic collisions for decreasing m/m_0 slows the relaxation of energy. As a consequence, Monte Carlo simulations require a large computation time while at the same time the statistical fluctuations deteriorate the accuracy of the output data. We see in the Fig. 1 that the error bars are increased for decreasing m/m_0.

For a fixed mass ratio we see that Q_L is increased monotonically with E/n_0. In this model, the elastic cross section is constant rendering collision frequency to be directly proportional to the square root of the charge particle energy. With the increase of E/n_0, the collision frequency also increases, but not enough to overcome the directed action of the force and the simultaneous increase of the mobility of charged particles (see Appendix B). As a consequence, Q_L rises with rising E/n_0. When it comes to Q_T, for the entire range of E/n_0 considered, it is found that $Q_T > 0$ (not shown here). This indicates that the absolute value of the sum of Q_{xxz} and Q_{xzx} is greater than the absolute value of the coefficient Q_{zxx}. In this model, $Q_{zxx} < 0$ since the collision frequency is directly proportional to the square root of charged-particle energy. The negative value of Q_{zxx} due to elastic collisions with a constant cross section has been observed for the Reid model gas at low
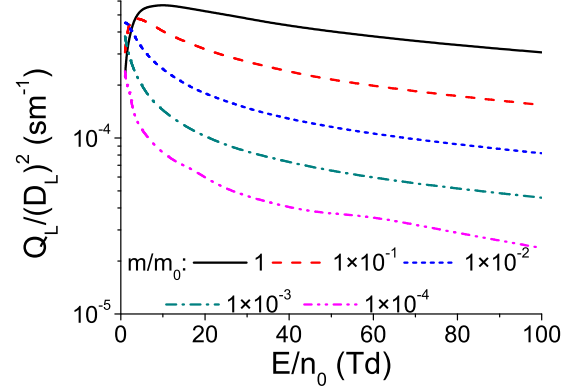

FIG. 2. Variation of the Q_L to D_L^2 ratio as a function of E/n_0 for the hard sphere model.

electric fields where the rate for inelastic collisions is negligible (see Sec. III D). Note that in our Monte Carlo simulations we are not able to evaluate the individual components Q_{xxz}, Q_{xzx} and Q_{zxx}, but only their sum [see Eq. (47)].

Figure 1 clearly illustrates that for decreasing m/m_0 the coefficients Q_L (and Q_T) are increased. It should be noted that for the hard sphere model the third-order transport coefficients scale with the factor $\frac{1}{\sqrt{m_0}} \left(\frac{m+m_0}{mA^2} \right)^{5/4}$ [19]. This raises an interesting question: does the spatial profile of the swarm deviate from a Gaussian distribution more for light charged particles, including electrons and/or positrons, or for more massive ions? In order to investigate this issue, in Figs. 2 and 3 we show the variation of the $\frac{1}{n_0} Q_L/D_L^3$ and Q_L/D_L^2 as a function of E/n_0, respectively, where D_L is the longitudinal diffusion coefficient. Recall that the asymmetric contribution to the spatial profile of the swarm along the field direction is represented by the two terms; the first term is proportional to Q_L/D_L^3, while the second one is proportional to Q_L/D_L^2 [see Eq. (33)]. We observe that both quantities $\frac{1}{n_0} Q_L/D_L^3$ and Q_L/D_L^2 are decreased with a decrease of m/m_0, which indicates that the contribution of the third-order transport coefficients to the spatial profile of the swarm becomes more significant for ions in comparison with electrons and/or positrons.
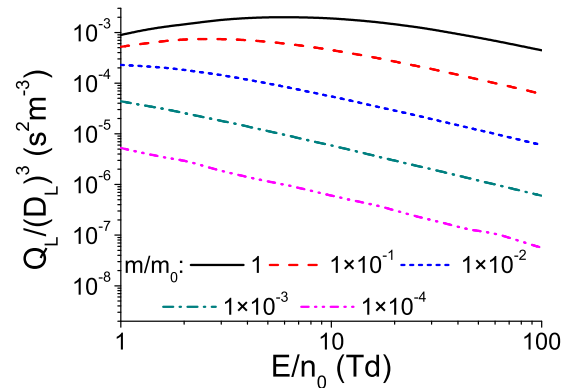

FIG. 3. Variation of the Q_L to D_L^3 ratio as a function of E/n_0 for the hard sphere model. Calculations are performed assuming the gas number density $n_0 = 3.54 \times 10^{22} \ \text{m}^{-3}$.
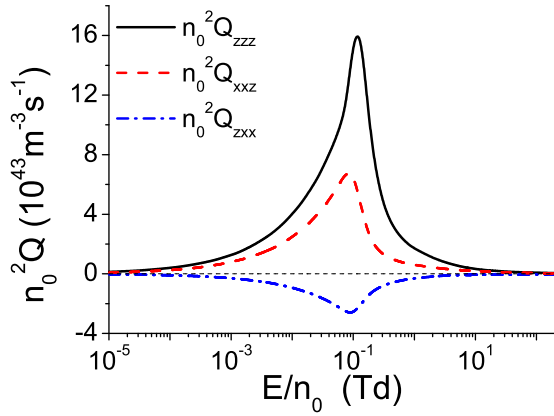
FIG. 4. Variation of the third-order transport coefficients with E/n_0 for the Reid ramp model. Calculations are performed via a multiterm theory for solving the Boltzmann equation.

D. The Reid ramp model

The Reid ramp inelastic model of interaction is given by [85]

$$\sigma_m(\epsilon) = 6 \text{ Å}^2 \quad \text{(elastic cross section)},$$

$$\sigma_{\text{inel}}(\epsilon) = \begin{cases} 10(\epsilon - 0.2) \text{ Å}^2, & \epsilon \geqslant 0.2 \text{ eV} \\ & \text{(inelastic cross section)}, \\ 0, & \epsilon < 0.2 \text{ eV} \end{cases}$$

$$m_0 = 4 \text{ amu},$$

$$T_0 = 0 \text{ K}, \tag{52}$$

where m_0 and T_0 represent the mass and temperature of the neutral gas particles while ϵ has the units of eV. Initially, this particular model was developed with the aim of testing the validity of the two-term approximation for solving the Boltzmann equation. Since the early work of Reid [85], the model has been used extensively as a benchmark for a variety of numerical techniques for solving the Boltzmann equation and Monte Carlo codes under steady-state [70–72,82,83] and time-dependent conditions [17,68]. In the present work we extend the model to consider the behavior of the individual elements of the third-order transport coefficient tensor in the presence of both electric and magnetic fields. Thus, the utility of the Reid ramp model in the present work is twofold: (1) it will enable us to determine the influence of an energy dependent collision frequency in addition to the influence of strong inelastic processes on the behavior of the third-order transport coefficients, and (2) it is a good test of the accuracy of the two-term approximation for solving Boltzmann's equation.

In Fig. 4 we show the variation of the coefficients Q_{zzz}, Q_{xxz}, and Q_{zxx} with the reduced electric field E/n_0. Over the range of E/n_0 considered, we see that Q_{zzz} and Q_{xxz} are positive while Q_{zxx} is negative. Such behavior of the third-order transport coefficients can be attributed to the fact that for the Reid ramp model the total collision frequency is a monotonically increasing function of the electron energy. Due to the increase of the total collision frequency over the entire range of E/n_0, Q_{zxx} is negative (see Appendix B). However, this increase is not significant enough to render Q_{zzz} and Q_{xxz} negative. In any case, the absolute values of
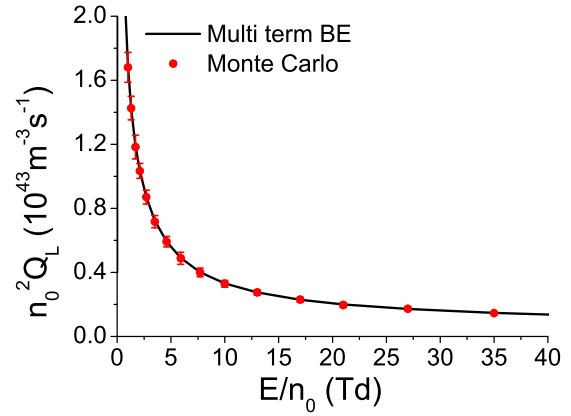

FIG. 5. Comparison between the multiterm Boltzmann equation results for longitudinal third-order transport coefficient and those calculated with a Monte Carlo simulation technique.

the third-order transport coefficients are increasing functions of E/n_0 until reaching the particular value of E/n_0 value for which the inelastic collisions begin to play a significant role. In this case, their direct effect is to enhance collisions and thereby reduce diffusion which in turn reduces the third-order transport coefficients. In the limit of the highest E/n_0, the third-order transport coefficients are significantly reduced and approach zero values.

In Figs. 5 and 6 we show the comparison between the Boltzmann equation and Monte Carlo results of Q_L and Q_T, respectively. The comparison is presented only for relatively higher values of E/n_0 where both Q_L and Q_T are monotonically decreasing functions of E/n_0. In the limit of lower values of E/n_0, the relaxation of energy is a very slow process and Monte Carlo simulations require large computation time. The results from the Monte Carlo simulations are consistent and agree very well with those predicted by the Boltzmann equation analysis, validating the theoretical method for solving the Boltzmann equation and numerical integrity of both methods of calculations.

In Fig. 7 the percentage differences in the third-order transport coefficients for the Reid ramp model, calculated using the two-term and the fully converged multiterm solutions
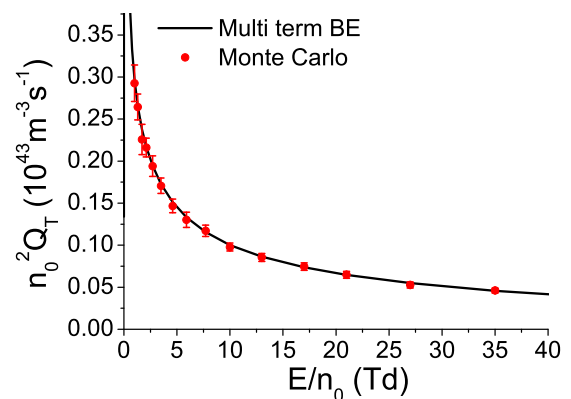

FIG. 6. Comparison between the multiterm Boltzmann equation results for transverse third-order transport coefficient and those calculated with a Monte Carlo simulation technique.
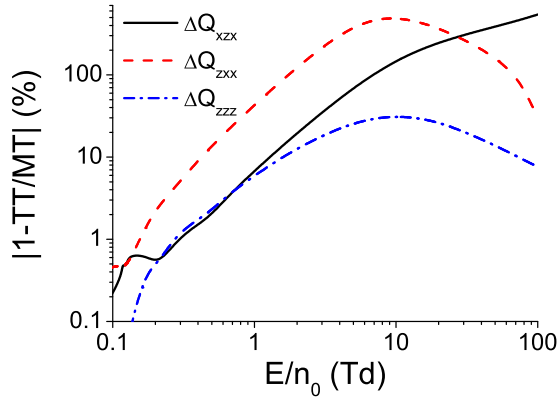
FIG. 7. Percentage difference between the two-term (TT) and multiterm (MT) results for the third-order transport coefficients for the Reid ramp model.
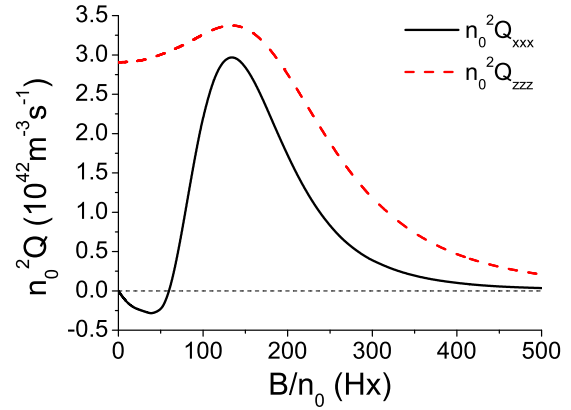

FIG. 8. Variation of $n_0^2 Q_{zzz}$ and $n_0^2 Q_{xxx}$ with B/n_0 for the Reid ramp model. Calculations are performed by a multiterm theory for solving the Boltzmann equation in a crossed field configuration. The reduced electric field E/n_0 is set to 12 Td.

of Boltzmann's equation, are shown. We see that maximum errors in the two-term approximation, for Q_{zzz} and Q_{zxx}, occur at about 10 Td where the mean energy of the electrons is close to the threshold of a cross section for inelastic collisions. On the other hand, the discrepancy between the two-term and multiterm solutions of Boltzmann's equation for Q_{xxz} increases with E/n_0 monotonically over the range of E/n_0 considered in this work. For the lower values of E/n_0, the coefficient Q_{zxx} appears to be the most sensitive with respect to the number of spherical harmonics used for solving Boltzmann's equation while for the higher values of E/n_0 the most sensitive coefficient is Q_{xzx}. We observe that the errors between the two-term and converged multiterm results can be as high as 500%. The presence of inelastic collisions produces asymmetry in velocity space which makes the two-term approximation inadequate for the analysis of the third-order transport coefficients. It is also important to note that the differences between the two-term approximation and multiterm solution of Boltzmann's equation for third-order transport coefficients are much higher than those for the lower-order transport coefficients, e.g., for the drift velocity and diffusion coefficients. This suggests that the third-order transport coefficients are more sensitive with respect to the way of solving the Boltzmann equation. Thus, it seems that the use of a multiterm theory for solving the Boltzmann equation is mandatory in the presence of inelastic collisions when it comes to calculations of the third-order transport coefficients.

In Fig. 8 we show the variation of the coefficients Q_{xxx} and Q_{zzz} as a function of B/n_0 at $E/n_0 = 12$ Td. As already discussed, Q_{zzz} describes the deviation from the Gaussian along the z axis (see Appendix B). For perpendicular electric and magnetic fields, Q_{xxx} is a measure of the deviation from the Gaussian along the $\mathbf{E} \times \mathbf{B}$ direction. For B/n_0 greater than approximately 150 Hx, we observe that both Q_{xxx} and Q_{zzz} monotonically decrease with increasing B/n_0. This is a clear indication of the magnetic-field-controlled regime in which the cyclotron frequency dominates the collision frequency and the electrons are held by the magnetic field lines. For B/n_0 less than approximately 150 Hx, the behavior of Q_{xxx} and Q_{zzz} is less intuitive. For these values of B/n_0 the collision

frequency is generally higher than the cyclotron frequency, but on average, an increasing magnetic field acts to increase the fraction of the orbit completed between collisions. As a consequence, the collision frequency begins to fall down with increasing B/n_0 and Q_{zzz} raises.

The behavior of Q_{xxx} for the lower values B/n_0 is particularly interesting. Initially, in the limit of the lowest B/n_0, Q_{xxx} is negative due to the Lorentz force and spatial variation of the energy (and hence spatial variation of the collision frequency), which on average induces the spatial variation of the average velocity of the electrons along the negative direction of the x axis. In this B/n_0 region, the negative sign of Q_{xxx} corresponds to an elongation of the swarm in the direction of the x component of the drift velocity (along the negative x axis in this field configuration). This is analogous to the elongation of the swarm described by the Q_{zzz} element along the z component of the drift velocity (the $q\mathbf{E}$ direction). With a further increase of B/n_0 the influence of collisions becomes more and more significant which in turn leads to the compressing or spreading of the swarm along the negative or positive direction of the x axis. Due to these effects Q_{xxx} becomes positive and increases with increasing B/n_0.

In Fig. 9 we show the remaining components of the third-order transport coefficient tensor as a function of B/n_0 for perpendicular electric and magnetic fields. For the higher values of B/n_0 all components decrease with an increasing B/n_0 as more and more electrons are held in their orbits by the magnetic field. For the lower values of B/n_0, however, the behavior of the third-order transport coefficients is complex due to many individual factors which simultaneously influence the third-order coefficient tensor. These individual factors include the thermal anisotropy (the chaotic motion of charged particles is different along different directions), magnetic anisotropy (the orientation of charged-particle orbits is controlled by the magnetic field), and spatial variations of the average velocity and average energy along the longitudinal and transverse directions. However, comparing the magnetic-field-free case and crossed electric and magnetic fields the interpretation of the third-order transport coefficients is similar (see Appendix B). For example, the coefficient Q_{zyy} describes
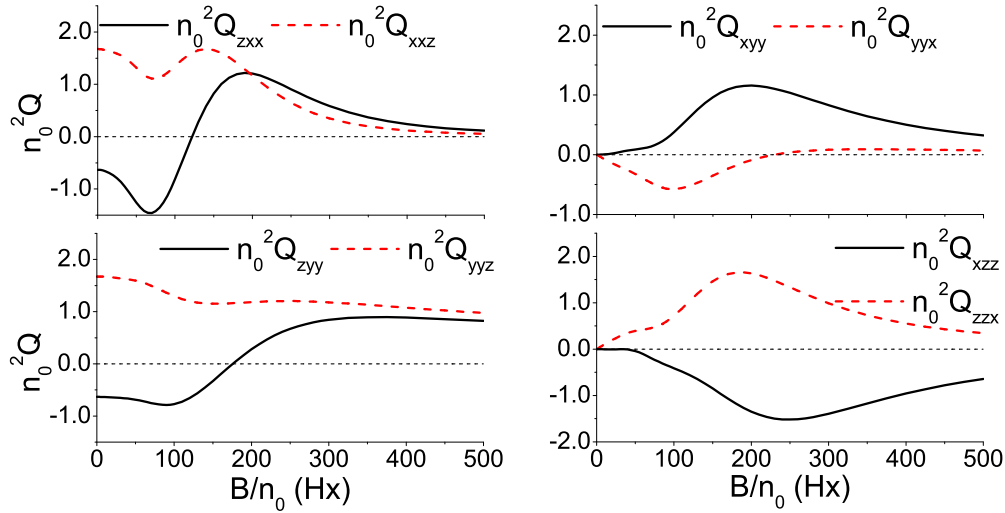
FIG. 9. Variation of the third-order transport coefficients with the repeated indices for the Reid ramp model. Calculations are performed via a multiterm theory for solving the Boltzmann equation in a crossed field configuration. The reduced electric field E/n_0 is set to 12 Td. The components of the $n_0^2 Q$ tensor are given in units of 10^{42} m^{-3}s^{-1}.

the differences in the longitudinal spreading in the central part of the swarm and along its transverse edges in the y direction. Likewise, the coefficient Q_{yyz} reflects the differences in the transverse spreading at the front of the swarm (along the direction given by the positive z) and at the trailing edge of the swarm (along the direction given by the negative z). The similar interpretation may be given for the remaining third-order transport coefficients shown in Fig. 9.

In Fig. 10 we show the comparison between the individual components of the third-order transport coefficient tensor, which could be identified in our Monte Carlo simulations, and the corresponding results, which are obtained from the numerical solution of the Boltzmann equation. The two sets

of results agree very well, even over the range of E/n_0 where the values of the coefficients are negative. We see that the error bars are not identical for different third-order transport coefficients. This indicates that the statistical fluctuations of the individual dynamical variables required for the evaluation of the third-order transport coefficients are not the same. Nevertheless, we see that the results obtained from the numerical solution of the Boltzmann equation are in very good agreement with those predicted by Monte Carlo simulations. This validates the theory and numerical scheme for solving the Boltzmann equation and Monte Carlo method when both the electric and magnetic fields are present and crossed at the right angle.
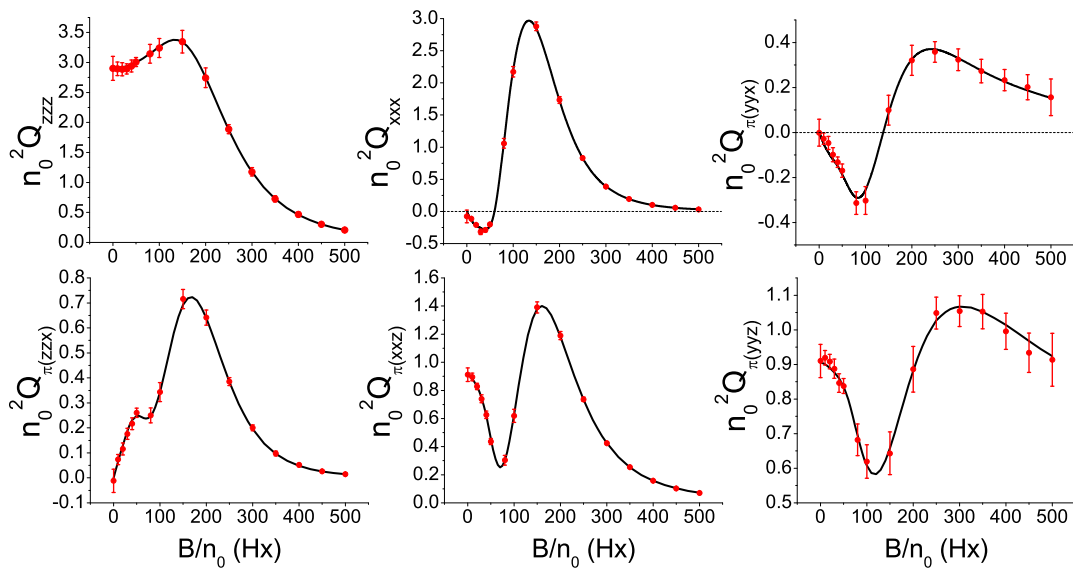

FIG. 10. Comparison between the multiterm Boltzmann equation results (full line) for various third-order transport coefficients and those calculated by a Monte Carlo simulation technique (symbols with error bars) in a crossed field configuration. The reduced electric field E/n_0 is set to 12 Td. The components of the $n_0^2 Q$ tensor are given in units of 10^{42} m^{-3}s^{-1}.
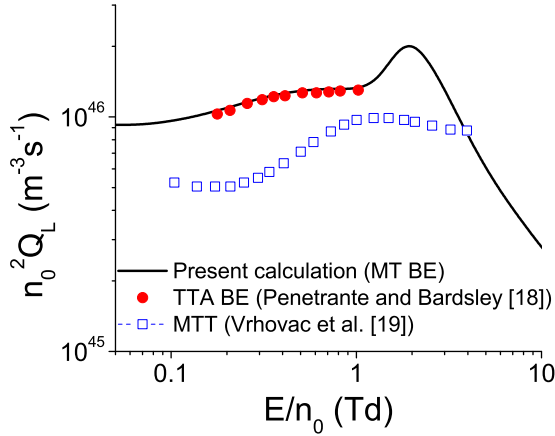
FIG. 11. Variation of the longitudinal third-order transport coefficient $n_0^2 Q_L$ with E/n_0 for electrons in neon. Our multiterm Boltzmann equation results (MT BE) are compared with those obtained by two-term approximation for solving the Boltzmann equation (TTA BE) [18] and momentum transfer theory (MTT) [19].

E. Third-order transport coefficients for electrons in neon

As an example of our calculations in real gases, in Fig. 11 we display the variation of the Q_L with E/n_0 for electrons in neon. The results obtained from the multiterm solution of the Boltzmann equation are compared with those predicted by the two-term approximation [18] and momentum transfer theory (MTT) [19]. The agreement between our multiterm results and those obtained by the two-term approximation is very good. This is a clear sign that there is no significant difference between the cross sections for elastic collisions of the electrons in neon used in the present multiterm calculations and in the previous two-term calculations performed by Penetrante and Bardsley [18]. The additional factor which favors the good agreement is the minimal influence of inelastic collisions. If inelastic collisions would play a more important role, then undoubtedly the differences between the multiterm and two-term results would be much higher. In any case, no calculations of Q_L were made by Penetrante and Bardsley for the higher values of E/n_0. On the other hand, the discrepancy between our results and those predicted by the momentum transfer theory (MTT) is clearly evident. This can be attributed to the fact that the momentum transfer theory assumes a very simple energy distribution function based on an effective mean energy. MTT produces reasonable results for the lowest-order transport coefficients such as drift velocity and even diffusion but it is expected to fail for ionization which depends on the high energy tail and also for higher-order transport coefficients that are very sensitive on the cross sections and correspondingly on the distribution function at all energies. Limitations of the MTT have been discussed many times [2,16,33,34,66].

In Fig. 12 we show the variation of the individual elements of the third-order transport coefficient tensor as a function of E/n_0 for electrons in neon. The same generic features of the third-order transport coefficients observed previously for the Reid ramp model are clearly evident. Both Q_{zzz} and Q_{xxz} are positive while the coefficient Q_{zxx} is negative over the range of E/n_0 considered. The total collision frequency
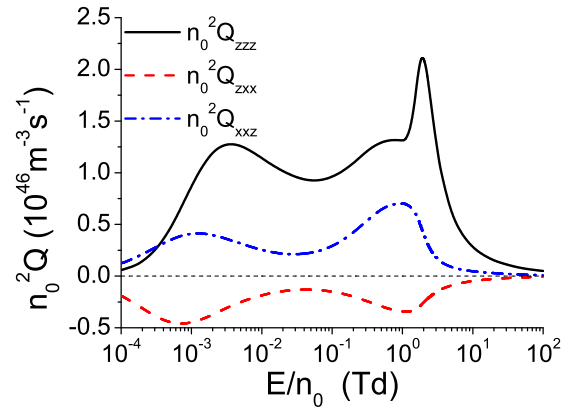

FIG. 12. Variation of the third-order transport coefficients with E/n_0 for electrons in neon. Calculations are performed using a multiterm approach for solving the Boltzmann equation.

increases with the increase of E/n_0, but not sufficiently fast to induced negative values of Q_{zzz} and Q_{xxz} (see Appendix B). The oscillatory behavior in the profiles of Q_{zzz}, Q_{xxz} and Q_{zzz} occurs for E/n_0 approximately less than 1 Td reflecting the energy variation of the cross section for elastic collisions. For E/n_0 approximately greater than 1 Td, inelastic collisions begin to play a significant role. As for the Reid ramp model, it appears that significant inelastic processes are required to suppress the longitudinal and transverse third-order transport coefficients.

IV. CONCLUSION

In this paper we have discussed the third-order transport coefficient tensor of charged-particle swarms moving in an infinite neutral gas under the influence of spatially homogeneous electric and magnetic fields. The third-order transport coefficient tensor is defined in terms of the extended flux gradient relation and the extended diffusion equation. The group projector method is then used for identifying the structure of the tensor and symmetries along its individual elements when both the electric and magnetic fields are present. For an electric-field-only situation, we have found that the third-order transport coefficient tensor has seven nonzero and only three independent elements. For parallel electric and magnetic fields, rotational invariance implies the third-order transport coefficient tensor has 11 nonzero and four independent elements, while for orthogonal electric and magnetic fields the tensor has 14 nonzero and 10 independent elements. Finally, when electric and magnetic fields are crossed at an arbitrary angle, it is found that the third-order transport coefficient tensor has 27 nonzero elements among which 18 are independent. The proposed methodology based on the group projector method and symmetry considerations of the Boltzmann equation can be applied to any of the transport coefficient of an arbitrary tensorial rank.

The second important issue addressed in the present work is the physical interpretation of the third-order transport coefficients. In order to resolve this issue, we have expanded the Fourier transform of the number charged-particle density in terms of the longitudinal and transverse third-order transport

coefficients. Using the inverse Fourier transformation of the expansion coefficients, we have derived the expression for the number density of charged particles in which the effects of third-order transport coefficients are explicitly included. It is found that deviations of the Gaussian distribution along the specific directions are directly related with the sign of the individual third-order transport coefficients.

Explicit expressions for the third-order transport coefficients in terms of the moments of the distribution function and in the absence of nonconservative collisions are derived in the framework of a multiterm theory for solving the Boltzmann equation. Using the symmetry properties of the moments, we have analyzed the structure of the third-order transport coefficient tensor. We have also developed the Monte Carlo method in which the third-order transport coefficients are defined in terms of the moments of charged-particle density in configuration space. It is found that only two independent components of the third-order transport coefficient tensor can be identified, as all tensor components are contracted with the corresponding spatial partial derivatives of charged-particle density. Thus, care must be taken when comparing the Monte Carlo results with those obtained by other theories.

Numerical calculations are performed using a multiterm solution of the Boltzmann equation for a range of model gases, including the Maxwell, hard sphere, and Reid ramp models. The results obtained are in very good agreement with those predicted by the Monte Carlo method when possible, over the range of the applied electric and magnetic fields. An important observation is that the contribution of the third-order transport coefficients to the spatial profile of the swarm becomes more pronounced for increasing the charged-particle to neutral-particle mass ratio. In this work we have also displayed and emphasized the need for a multiterm solution technique of Boltzmann's equation. It is found that the discrepancy between the two-term and fully converged multiterm results are much higher for the third-order transport coefficients than those for the lower order transport coefficients, e.g., drift velocity and diffusion coefficients. The theory and associated computer codes in the present work are equally valid for real gases. The third-order transport coefficients are calculated for electrons in neon and the results of calculations are compared with those evaluated by the two-term approximation for solving the Boltzmann equation and momentum transfer theory. Comparison with previous theories have shown surprisingly good agreement with the two-term solution of the Boltzmann equation and a significant disagreement with the momentum transfer theory.

The duality of transport coefficients, e.g., the existence of two different families of transport coefficients, the bulk and the flux, is well known in the presence of nonconservative collisions. Third-order transport coefficients are expected to be more sensitive to the explicit influence of nonconservative collisions. In order to investigate the effects of nonconservative collisions on the third-order transport coefficients one must go to third-order in the density gradient expansion to account for such effects. This remains the focus of our future investigation. Likewise, the remaining step to be taken, is to apply the theory and mathematical machinery developed in this work to investigate the correlation between the third-order transport coefficients and those of lower order, e.g., the drift and diffusion coefficients [19]. Additional issues which should be considered are the effects of anisotropic scattering and the behavior of the third-order transport coefficients in time-dependent electric and magnetic fields. Finally, it would be very challenging to model strong nonequilibrium systems such as streamer discharges by suitable coupling of the extended diffusion equation which incorporates the third-order transport coefficients for both the electrons and ions, and Poisson's equation for the space charge electric field calculation.

The theory presented here covers the structure, symmetries, and method of calculation of the third-order transport coefficients and the advantages that it may bring should it be applied. In this paper, we focus on physics of ionized gases (swarms and low-temperature collisional plasmas), but approach may be extended to other physical systems if one accounts for the dominant physical interactions and expected symmetries. One such example where these results may be applied directly is modeling of positron thermalization in gas filled traps [86,87] or thermalization of positrons in gases [88–90].

APPENDIX A: THE GROUP PROJECTOR METHOD

The structure of tensorial transport coefficients can be determined by employing group theory, since their structure reflects the symmetry of the system. The studied system consists of a swarm of charged particles, neutral background gas particles and the applied electric and magnetic fields. The symmetry group of a system is the group of all transformations under which the system is invariant [91–93]. The symmetry groups of the electric and magnetic fields are $C_{\infty V}$ and $C_{\infty h}$ respectively, since the electric field is a polar vector, and the magnetic field is an axial vector. These are the symmetry groups of an immobile cone and of a rotating cylinder, respectively [91]. If both electric and magnetic fields are present in the system, the symmetry group of the field configuration is determined by the angle between the fields. The symmetry group of the parallel fields configuration is C_∞. This is the symmetry group of a rotating cone [91]. Orthogonal field configuration has the symmetry group C_{1v}. The symmetry group of the general field configuration is the trivial group C_1. Background gas is invariant under all transformations from the orthogonal group $O(3)$. This is the symmetry group of a sphere. Therefore, the symmetry group of the field configuration is also the symmetry group of the entire system.

The structure of a tensor can be determined from its invariance, under operations from the symmetry group of the system. The action of a group G on vectors, from a vector space H, is represented by a group homomorphism from G to the general linear group on H, $GL(H)$ [92,93]. Polar

vectors, such as drift velocity, are transformed by the polar vector representation of the symmetry group of the system $D^{pv}(G)$. This representation is reducible [65,93] and, for finite and compact groups, it decomposes into the irreducible components $D^{(\mu)}(G)$ as

$$D^{pv}(G) = \oplus_{\mu=1}^{r} a_\mu D^{(\mu)}(G). \tag{A1}$$

Here a_μ is the number of times the irreducible representation $D^{(\mu)}(G)$ appears in the decomposition of $D^{pv}(G)$, and r is the number of inequivalent irreducible representations of the group G. In addition, for decomposable representations there exists a symmetry-adapted basis [65,93], which satisfies the condition

$$D^{pv}(G)|\mu t_\mu m\rangle = \sum_{n=1}^{|\mu|} D_{nm}^{(\mu)}(G)|\mu t_\mu n\rangle. \tag{A2}$$

This implies that for every irreducible representation $D^{(\mu)}(G)$ from (A1) there will be a subspace in H which transforms by $D^{(\mu)}(G)$ [65,93]. A very important representation, which exists for every group G, is the trivial irreducible representation A_0. This representation is defined as $D^{(A_0)}(g) = 1$, $\forall g \in G$. This representation is irreducible, since it is one dimensional.

It can be seen from (A2) that a vector is invariant under the action of $D^{(pv)}(G)$ if it belongs to the subspace of the trivial irreducible representation. This invariant subspace can be found by employing group projectors. In the case of the trivial representation, the group projector is simply

$$P^{(A_0)}(D^{pv}, G) = \frac{1}{|G|} \sum_{g \in G} D^{pv}(g) \tag{A3}$$

for finite groups, where $|G|$ is the order of the group G [65]. For one-parameter Lie groups the group projector for A_0 is

$$P^{(A_0)}(D^{pv}, G) = \sum_R \int D^{pv}(R)\, dR. \tag{A4}$$

Here the summation goes over distinct connected components, and integration is taken over the range of the group parameter [93]. Any vector, from the invariant subspace of $D^{pv}(G)$, including the drift velocity, is a linear combination of the eigenvectors of the projection operator $P^{(A_0)}(D^{pv}, G)$.

Diffusion tensor is a linear operator which maps the local density gradient vector $\nabla n(\mathbf{r}, t)$ onto the diffusive flux vector. Therefore diffusion tensor belongs to the range of the projector $P^{(A_0)}(D^{pv\otimes 2}, G)$ where $D^{pv\otimes 2}(G)$ represents $D^{pv} \otimes D^{pv}(G) = D^{pv}(G) \otimes D^{pv}(G)$. Similarly the skewness tensor maps the tensor square of the gradient vector, which acts upon the local density $\nabla \otimes \nabla n(\mathbf{r}, t)$, onto the vector of the third-order diffusive flux. Thus the skewness tensor belongs to the range of the projection operator $P^{(A_0)}(D^{pv} \otimes [D^{pv}]^2, G)$, where $[D^{pv}]^2$ represents the symmetrized tensor square of the polar vector representation. This symmetrization is a result of the commutativity of the gradient operators.

Strictly speaking, the action of the group on operators, such as diffusion tensor and skewness tensor, is represented by employing superoperators [94]. They are defined as $\widehat{\widehat{D}}(g)\hat{A} = D^{pv}(g)\hat{A}D^{pv}(g^{-1})$. Therefore, the most straightforward application of group theory would require the use of group superoperators. However, this is not necessary, since every

second rank basis operator $|i\rangle \otimes \langle j|$ acting on a vector space H is uniquely paired with a basis vector $|i\rangle \otimes |j\rangle$ from the vector space $H \otimes H$. The same applies for the basis operators of the third rank $|i\rangle \otimes [\langle j| \otimes \langle k|]$ and basis vectors $|i\rangle \otimes [|j\rangle \otimes |k\rangle]$ from the vector space $H \otimes [H \otimes H]$. Here square brackets represent symmetrization of the tensor product. Thus, the group projector method can be applied for representations $D^{pv}(G) \otimes D^{pv}(G)$ and $D^{pv} \otimes [D^{pv}]^2$ in the corresponding vector spaces. Then eigenvectors of the group projectors can be mapped into the corresponding basis tensors. Therefore diffusion tensor and skewness tensor are linear combinations of the basis tensors, which are obtained from eigenvectors of the projection operators $P^{(A_0)}(D^{pv} \otimes D^{pv}, G)$ and $P^{(A_0)}(D^{pv} \otimes [D^{pv}]^2, G)$, respectively. Moreover, it is not necessary to use $D^{pv} \otimes [D^{pv}]^2$ for determining the structure of the skewness tensor. One can instead use $D^{pv} \otimes D^{pv} \otimes D^{pv}$ and symmetrize the resulting tensors by the last two indices.

APPENDIX B: PHYSICAL INTERPRETATION OF THE INDIVIDUAL COMPONENTS OF THE THIRD-ORDER TRANSPORT COEFFICIENT TENSOR AND ANALYSIS OF THEIR SIGN

Using the flux gradient relation (7), the fluxes of charged particles induced exclusively by the third-order transport coefficient tensor are given by

$$\Gamma_{Q,z} = Q_{zzz}\frac{\partial^2 n(\mathbf{r}, t)}{\partial z^2} + Q_{zxx}\left[\frac{\partial^2 n(\mathbf{r}, t)}{\partial x^2} + \frac{\partial^2 n(\mathbf{r}, t)}{\partial y^2}\right],$$

$$\Gamma_{Q,x} = 2Q_{xxz}\frac{\partial^2 n(\mathbf{r}, t)}{\partial x \partial z}, \tag{B1}$$

where Q_{zzz}, Q_{zxx}, and Q_{xxz} are independent components of the third-order transport coefficient tensor (see Sec. II B). The leading term in the expansion of the density of charged particles (33) is of key importance in considering the sign of the derivative of the charged-particle density. Therefore, in what follows we consider only this term in the analysis of the fluxes of charged particles (B1). The second-order derivatives of the Gaussian (32) are given by

$$\frac{\partial^2 n^{(0)}(\mathbf{r}, t)}{(\partial z)^2} = \left(z^2 - \sigma_z^2\right)\frac{n^{(0)}(\mathbf{r}, t)}{\sigma_z^4}, \tag{B2}$$

$$\frac{\partial^2 n^{(0)}(\mathbf{r}, t)}{(\partial x)^2} = \left(x^2 - \sigma_x^2\right)\frac{n^{(0)}(\mathbf{r}, t)}{\sigma_x^4}, \tag{B3}$$

$$\frac{\partial^2 n^{(0)}(\mathbf{r}, t)}{(\partial x \partial z)} = xz\frac{n^{(0)}(\mathbf{r}, t)}{\sigma_x^2 \sigma_z^2}, \tag{B4}$$

where

$$\sigma_x^2 = 2D_T t, \quad \sigma_z^2 = 2D_L t. \tag{B5}$$

For simplicity, the above derivatives correspond to the coordinate system whose origin is placed at the center of the Gaussian distribution. Thus, the term $z - Wt$ is replaced by the term z in (B2) and (B4).

In order to visualize these second-order derivatives in the most efficient way for arbitrarily values of σ_z, we introduce the set of new coordinates $x/\sigma_x = \chi_x$, $y/\sigma_y = \chi_y$, and $z/\sigma_z = \chi_z$.
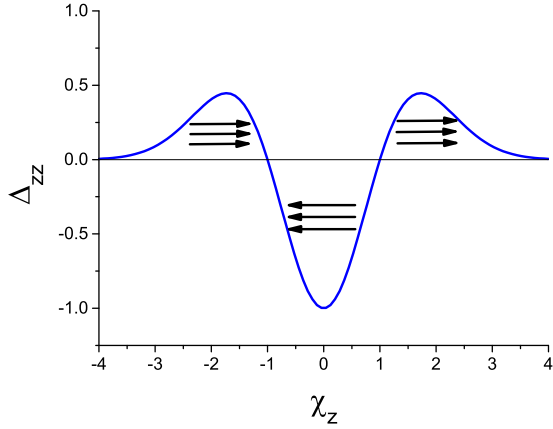
FIG. 13. The normalized derivative Δ_{zz} of the density of charged particles as a function of the relative coordinate χ_z. The arrows denote the direction of motion represented by Q_{zzz} if this component is positive. The field force is oriented along the positive χ_z direction.

Using the new coordinates, Eqs. (B2)–(B4) become

$$\frac{\partial^2 n^{(0)}}{\partial \chi_z^2} = (\chi_z^2 - 1)n^{(0)}, \tag{B6}$$

$$\frac{\partial^2 n^{(0)}}{\partial \chi_x^2} = (\chi_x^2 - 1)n^{(0)}, \tag{B7}$$

$$\frac{\partial^2 n^{(0)}}{\partial \chi_x \partial \chi_z} = \chi_x \chi_z n^{(0)}, \tag{B8}$$

where

$$n^{(0)}(\boldsymbol{\chi}, t) = C_\chi \exp\left[-\frac{1}{2}\left(\chi_z^2 + \chi_x^2 + \chi_y^2\right)\right] \tag{B9}$$

and

$$C_\chi = \frac{N_0 e^{-R_{\text{net}}t}}{(2\pi)^{3/2}\sigma_x^2\sigma_z}. \tag{B10}$$

By combining equations (B6)–(B10) the normalized second-order derivatives of the density of charged particles can be written as follows:

$$\Delta_{zz} \equiv \frac{1}{C_\chi}\frac{\partial^2 n^{(0)}}{\partial \chi_z^2} = (\chi_z^2 - 1)e^{-\frac{1}{2}(\chi_z^2 + \chi_x^2 + \chi_y^2)}, \tag{B11}$$

$$\Delta_{xx} \equiv \frac{1}{C_\chi}\frac{\partial^2 n^{(0)}}{\partial \chi_x^2} = (\chi_x^2 - 1)e^{-\frac{1}{2}(\chi_z^2 + \chi_x^2 + \chi_y^2)}, \tag{B12}$$

$$\Delta_{xz} \equiv \frac{1}{C_\chi}\frac{\partial^2 n^{(0)}}{\partial \chi_x \partial \chi_z} = \chi_x \chi_z e^{-\frac{1}{2}(\chi_z^2 + \chi_x^2 + \chi_y^2)}. \tag{B13}$$

In Fig. 13 we show the quantity Δ_{zz} as a function of χ_z. We see that the representing curve is symmetric with respect to the origin in which it has a minimum. If Q_{zzz} is positive the direction of motion represented by this component depends on the sign of Δ_{zz} in the following way. When Δ_{zz} is positive, the motion described by Q_{zzz} is also directed along the positive z axis, which is indicated by arrows that are oriented to the right. Conversely, when Δ_{zz} is negative, the motion described by Q_{zzz} is directed along the negative z axis, which is indicated in this case by arrows that are oriented to the left. Therefore, when $Q_{zzz} > 0$ the leading edge of the Gaussian is elongated while the training edge is compressed to a certain extent. It is
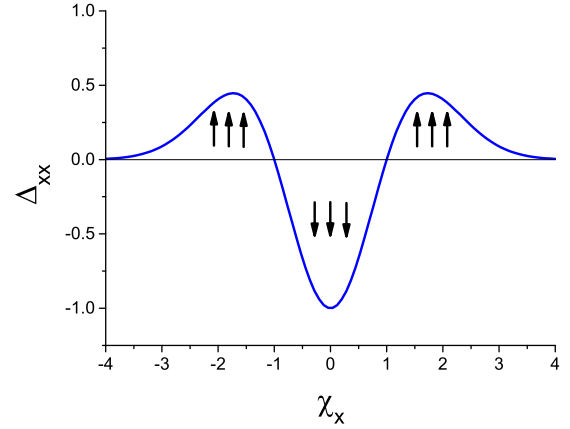

FIG. 14. The normalized derivative Δ_{xx} of the density of charged particles as a function of the relative coordinate χ_x. The arrows denote the direction of motion represented by Q_{zxx} if this component is positive: the arrows directed upwards (downwards) represent motion in the positive (negative) z direction.

clear that when $Q_{zzz} < 0$, then the opposite situation holds: the leading edge of the Gaussian is compressed while the trailing edge is elongated.

Figure 14 shows the graph of the function Δ_{xx}. This function is identical to the one illustrated in Fig. 13. When Q_{zxx} is positive, the motion described by Q_{zxx} is directed along the positive z axis at the swarm edges, which is indicated by arrows that are oriented upwards. However, the motion represented by Q_{zxx} at the swarm center is directed along the negative z axis in this case, which is indicated by arrows that are oriented downwards. Likewise, if Q_{zxx} is negative, then the motion described by Q_{zxx} is directed along the negative z axis at the edges of the swarm, and along the positive z axis at the swarm center.

In Fig. 15 we show the contour plot of the function Δ_{xz} as a function of χ_x and χ_z. This function is positive in the first and

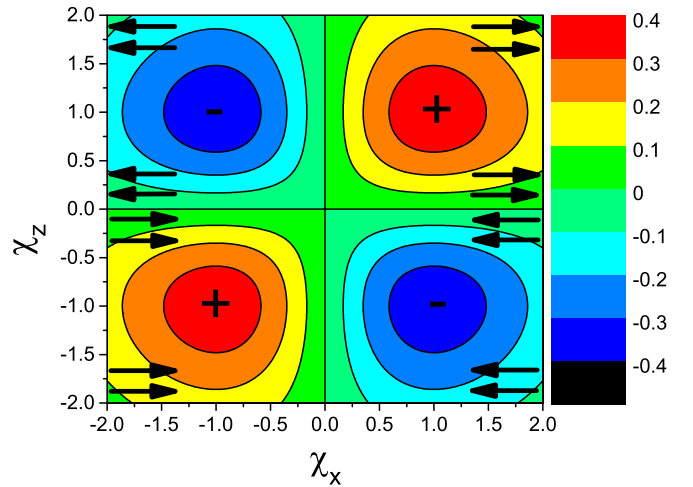FIG. 15. The normalized derivative Δ_{xz} of the density of charged particles as a function of the relative coordinates χ_x and χ_z. The arrows denote the direction of motion represented by Q_{xxz} if this component is positive.

third quadrant and negative in the second and fourth quadrant. If Q_{xxz} is positive the direction of motion represented by this component depends on the sign of Δ_{xz} in the following way. When Δ_{xz} is positive the motion described by Q_{xxz} is directed along the positive x axis which is indicated by arrows that are oriented to the right. Conversely, when Δ_{xz} is negative the motion described by Q_{xxz} is directed along the negative x axis which is indicated by arrows that are oriented to the left. It is clear that when $Q_{xxz} < 0$ the direction of motion represented by this component is reversed. It should be noted that the joint contribution of Q_{zxx} and Q_{xxz} leads to a pear-shaped Gaussian distribution.

In what follows we investigate the effects of the gas pressure on the third-order transport coefficients. Using the set of new coordinates χ_x, χ_y and χ_z, the number density of charged particles given by Eq. (33) can be written as

$$n^{(1)}(\boldsymbol{r}, t) = n^{(0)}(\boldsymbol{r}, t) \left[1 + \frac{tQ_L}{\sigma_z^3} \chi_z (\chi_z^2 - 3) + \frac{3tQ_T}{\sigma_x^2 \sigma_z} \chi_z (\chi_x^2 + \chi_y^2 - 2) \right]. \quad \text{(B14)}$$

From Eq. (B14) we see that the contribution of the third-order transport coefficients to the spatial profile of the swarm is reduced with increasing number density of the neutral particles n_0. This is due to the fact that Q_L and Q_T scale as $1/n_0^2$ while σ_x and σ_z scale as $1/\sqrt{n_0}$ with the variation of n_0. From this, it follows that the terms tQ_L/σ_z^3 and $3tQ_T/\sigma_x^2 \sigma_z$ scale as $1/\sqrt{n_0}$ with with the variation of n_0. In addition, from Eq. (B14) we can also see that the influence of the third-order transport coefficients on the spatial profile of charged particles is reduced as $1/\sqrt{t}$ with increasing t due to the time dependence of the terms tQ_L/σ_z^3 and $3tQ_T/\sigma_x^2 \sigma_z$. Thus, from the scalings of the third-order transport coefficients and associated properties it can be concluded that their experimental determination would be the most efficient at low pressures. On the other hand, measurements at low pressures in drift tubes require optimal gaps and volumes in order to reach the conditions where hydrodynamic approximation is applicable (negligible length or relaxation distances as compared to the overall gap). Special care should be taken in order to avoid kinetic phenomena [16] such as diffusion cooling [95,96] and other issues associated with an inability of the swarm to be fully relaxed due to a small number of collisions of charged particles and neutral gas particles. In any case, the experimental determination of third-order transport coefficients requires large gas volumes and low pressures. Similar findings have been reported in Ref. [18].

In studies of third-order transport coefficients tensor we often find it necessary to refer to the sign of the third-order transport coefficients to explain certain phenomena. Let us assume that the swarm of charged particles is acted on solely by an electric field. The following elementary considerations apply.

The motion of charged particles represented by the longitudinal component Q_{zzz} produces differences in the spreading of the density profile between the front and trailing edges of the swarm. When $Q_{zzz} > 0$, the front edge of the density profile is elongated, while the trailing edge is compressed. The opposite

situation holds when $Q_{zzz} < 0$: the front edge of the swarm is compressed while the trailing edge of the profile is elongated.

Charged particles at the front of the swarm have higher energies on average, than those at the back of the swarm, as they are accelerated through the larger potential difference. If the collision frequency is independent of energy, the spread of charged particles along the field direction is induced by the action of the force and by the chaotic motion of particles. If the collision frequency is a decreasing function of the charged-particle energy, the friction due to collisions along the field direction is also decreased contributing additionally in the spreading of the density profile. When collision frequency increases with the particle energy, however, the friction will be enhanced along the field direction which in turn reduces the spreading of the density profile. Thus, the longitudinal component Q_{zzz} is positive whenever the growth of collision frequency and associated energy losses in collisions are not able to affect the spreading of charged particles due to the electric field force and chaotic motion of charged particles. This is exactly what happens in most cases considered in our calculations.

The motion of a swarm represented by Q_{xzx} produces differences in the transverse spreading of the density profile. When $Q_{xzx} > 0$, the density profile is expanded along the transverse direction at the front of the swarm while at the back of the swarm the profile is compressed. When $Q_{xzx} < 0$, the density profile is compressed along the transverse direction at the front and extended at the trailing edge of the swarm.

The electric force does not act along the transverse direction. This suggests that the spreading of the density profile is entirely controlled by the chaotic motion of charged particles. If the collision frequency decreases with energy, this will further enhance the transverse spread at the front of the swarm as collisions between charged particles and background gas molecules are less frequent. If the collision frequency increases with energy, the reverse situation occurs. In this case it is the high energy electrons, which predominantly exist at the front of the swarm, have more collisions than those at the back of the swarm. This results in a greater resistance to the transverse spreading at the front of the swarm. Thus, the transverse component Q_{xzx} is positive under conditions in which the growth of the collision frequency and energy losses in collisions are not intensive enough to exceed the higher average speed of charged particles at the front of the swarm.

The off-diagonal component Q_{zxx} describes the differences in the longitudinal spreading in the central part of the swarm and along its transverse edges. If $Q_{zxx} > 0$, the longitudinal spreading is faster at the transverse edges than in the central part of the swarm. Conversely, if $Q_{zxx} < 0$, the reverse situation occurs: the longitudinal spreading is more pronounced in the central part of the swarm than at the edges. The parabolic rise in mean energy along the transverse direction favors the faster longitudinal spreading at the transverse edges of the swarm. The parabolic rise in mean energy is due to the fact that the most energetic electrons quickly cross the distance between the swarm's center and its edges, if the increase of the collision frequency is not large enough to compensate for the high speed of energetic electrons. If the collision frequency is independent of energy, this is the only contribution to the difference in the rate of longitudinal expansion along

TABLE II. Symmetry properties of the individual components of the skewness tensor. The transformation represents A (parity), B (rotation of π about the z axis), C (parity and rotation of π about the y axis), and D (parity and rotation of π about the x axis).

Tensor component	$\boldsymbol{E} \to -\boldsymbol{E}, \boldsymbol{B} \to \boldsymbol{B}$	$\boldsymbol{E} \to \boldsymbol{E}, \boldsymbol{B} \to (-B_y, B_z)$	$\boldsymbol{E} \to \boldsymbol{E}, \boldsymbol{B} \to (B_y, -B_z)$	$\boldsymbol{E} \to \boldsymbol{E}, \boldsymbol{B} \to -\boldsymbol{B}$
		Transformation		
Q_{xxz}, Q_{xzx}	$-Q_{xxz}, -Q_{xzx}$	Q_{xxz}, Q_{xzx}	Q_{xxz}, Q_{xzx}	Q_{xxz}, Q_{xzx}
Q_{yyz}, Q_{yzy}	$-Q_{yyz}, -Q_{yzy}$	Q_{yyz}, Q_{yzy}	Q_{yyz}, Q_{yzy}	Q_{yyz}, Q_{yzy}
Q_{zxx}	$-Q_{zxx}$	Q_{zxx}	Q_{zxx}	Q_{zxx}
Q_{zyy}	$-Q_{zyy}$	Q_{zyy}	Q_{zyy}	Q_{zyy}
Q_{zzz}	$-Q_{zzz}$	Q_{zzz}	Q_{zzz}	Q_{zzz}
Q_{xxx}	$-Q_{xxx}$	$-Q_{xxx}$	Q_{xxx}	$-Q_{xxx}$
Q_{xyy}	$-Q_{xyy}$	$-Q_{xyy}$	Q_{xyy}	$-Q_{xyy}$
Q_{xzz}	$-Q_{xzz}$	$-Q_{xzz}$	Q_{xzz}	$-Q_{xyy}$
Q_{yxy}, Q_{yyx}	$-Q_{yxy}, -Q_{yyx}$	$-Q_{yxy}, -Q_{yyx}$	Q_{yxy}, Q_{yyx}	$-Q_{yxy}, -Q_{yyx}$
Q_{zxz}, Q_{zzx}	$-Q_{zxz}, -Q_{zzx}$	$-Q_{zxz}, -Q_{zzx}$	Q_{zxz}, Q_{zzx}	$-Q_{zxz}, -Q_{zzx}$
Q_{xyz}, Q_{xzy}	$-Q_{xyz}, -Q_{xzy}$	Q_{xyz}, Q_{xzy}	$-Q_{xyz}, -Q_{xzy}$	$-Q_{xyz}, -Q_{xzy}$
Q_{yxz}, Q_{yzx}	$-Q_{yxz}, -Q_{yzx}$	Q_{yxz}, Q_{yzx}	$-Q_{yxz}, -Q_{yzx}$	$-Q_{yxz}, -Q_{yzx}$
Q_{zxy}, Q_{zyx}	$-Q_{zxy}, -Q_{zyx}$	Q_{zxy}, Q_{zyx}	$-Q_{zxy}, -Q_{zyx}$	$-Q_{zxy}, -Q_{zyx}$
Q_{xxy}, Q_{xyx}	$-Q_{xxy}, -Q_{xyx}$	$-Q_{xxy}, -Q_{xyx}$	$-Q_{xxy}, -Q_{xyx}$	Q_{xxy}, Q_{xyx}
Q_{yxx}	$-Q_{yxx}$	$-Q_{yxx}$	$-Q_{yxx}$	Q_{yxx}
Q_{yyy}	$-Q_{yyy}$	$-Q_{yyy}$	$-Q_{yyy}$	Q_{yyy}
Q_{yzz}	$-Q_{yzz}$	$-Q_{yzz}$	$-Q_{yzz}$	Q_{yzz}
Q_{yz}, Q_{zzy}	$-Q_{zyz}, -Q_{zzy}$	$-Q_{zyz}, -Q_{zzy}$	$-Q_{zyz}, -Q_{zzy}$	Q_{zyz}, Q_{zzy}

the transverse direction. If the collision frequency decreases with energy, this is an additional factor which contributes to the rapid longitudinal spread at the transverse edges of the swarm. If the collision frequency increases with energy, this contributes to greater resistance to longitudinal expansion at the transverse edges than in the center of the swarm. For a constant collision frequency, Q_{zxx} component is positive, but much less in comparison to Q_{zzz} and Q_{xzx}. If the collision frequency decreases with energy, this component is positive and greater in magnitude than in the previous case. If the collision frequency increases with energy and Q_{xzx} is positive then the Q_{zxx} component is negative. This could be

expected, since the particles at the transverse edges have a slightly higher energy, and thus higher collision frequency. Such behavior of Q_{zxx} has been observed in the case of electron swarms in most atomic and molecular gases. If the collision frequency increases with energy and Q_{xzx} is negative then Q_{zxx} is positive. A possible explanation for this effect is that when Q_{xzx} is negative the energy of the electrons at the transverse edges of the swarm is, on average, less than in the center of the swarm. The high-energy electrons undergo more and more collisions for increasing electron energy which in turn prevent them from reaching the transverse edges of the swarm.

APPENDIX C: EXPRESSIONS FOR THE INDIVIDUAL ELEMENTS OF THE THIRD-ORDER TRANSPORT COEFFICIENT TENSOR IN THE BOLTZMANN EQUATION ANALYSIS AND MONTE CARLO SIMULATIONS

Using symmetry properties of the moments $F(\nu lm|s\lambda\mu)$ discussed in Ref. [70], the corresponding symmetry properties of the individual elements of the third-order transport coefficient tensor are detailed in Table II. The structure of the tensor may be determined by applying the symmetries in Table II in combination with the additional physical arguments that concern fluxes of charged particles induced by magnetic field. These arguments are necessary to identify the zero elements as well as those elements of the tensor which are equal between each other for a given configuration of the fields. The similar procedure has been applied for the vectorial and tensorial transport coefficients of the lower order [70].

In this Appendix we present the explicit expressions for the individual elements of the flux third-order transport coefficient tensor. These expressions have been derived by considering the flux-gradient relation in the spherical form (41) and explicit expressions for the irreducible gradient tensor operator [33]. In the following expressions α is omitted from the argument of F for brevity.

For parallel electric and magnetic fields, the individual elements of the flux tensor are given by

$$Q_{xxz} = \frac{1}{\sqrt{2}\alpha}[\text{Im}(F(011|221)) - \text{Im}(F(01-1|221))], \tag{C1}$$

$$Q_{xyz} = \frac{1}{\sqrt{2}\alpha}[\text{Re}(F(01-1|221)) - \text{Re}(F(011|221))], \tag{C2}$$

$$Q_{zxx} = -\frac{1}{\alpha}\left[\frac{1}{\sqrt{3}}\text{Im}(F(010|200)) + \frac{1}{\sqrt{6}}\text{Im}(F(010|220))\right] + \frac{1}{\alpha}\text{Im}(F(010|222)), \tag{C3}$$

$$Q_{zzz} = \frac{1}{\alpha}\left[\sqrt{\frac{2}{3}}\text{Im}(F(010|220)) - \frac{1}{\sqrt{3}}\text{Im}(F(010|200))\right]. \tag{C4}$$

For perpendicular electric and magnetic fields, the individual elements of the flux tensor are given by

$$Q_{xxx} = \frac{\sqrt{2}}{\alpha}\left[\frac{1}{\sqrt{3}}\text{Im}(F(011|200)) + \frac{1}{\sqrt{6}}\text{Im}(F(011|220))\right] + \frac{1}{\sqrt{2}\alpha}[-\text{Im}(F(011|222)) + \text{Im}(F(01-1|222))], \tag{C5}$$

$$Q_{xyy} = \frac{\sqrt{2}}{\alpha}\left[\frac{1}{\sqrt{3}}\text{Im}(F(011|200)) + \frac{1}{\sqrt{6}}\text{Im}(F(011|220))\right] + \frac{1}{\sqrt{2}\alpha}[\text{Im}(F(011|222)) - \text{Im}(F(01-1|222))], \tag{C6}$$

$$Q_{xzz} = \frac{\sqrt{2}}{\alpha}\left[\frac{1}{\sqrt{3}}\text{Im}(F(011|200)) - \sqrt{\frac{2}{3}}\text{Im}(F(011|220))\right], \tag{C7}$$

$$Q_{xxz} = \frac{1}{\sqrt{2}\alpha(t)}[\text{Im}(F(011|221)) - \text{Im}(F(01-1|221))], \tag{C8}$$

$$Q_{yxy} = -\frac{1}{\sqrt{2}\alpha}[\text{Im}(F(011|222))+\text{Im}(F(01-1|222))], \tag{C9}$$

$$Q_{yyz} = \frac{1}{\sqrt{2}\alpha}[\text{Im}(F(011|221))+\text{Im}(F(01-1|221))], \tag{C10}$$

$$Q_{zxz} = -\frac{1}{\alpha}\text{Im}(F(010|221)), \tag{C11}$$

$$Q_{zxx} = -\frac{1}{\alpha}\left[\frac{1}{\sqrt{3}}\text{Im}(F(010|200)) + \frac{1}{\sqrt{6}}\text{Im}(F(010|220))\right] + \frac{1}{\alpha}\text{Im}(F(010|222)), \tag{C12}$$

$$Q_{zyy} = -\frac{1}{\alpha}\left[\frac{1}{\sqrt{3}}\text{Im}(F(010|200)) + \frac{1}{\sqrt{6}}\text{Im}(F(010|220))\right] - \frac{1}{\alpha}\text{Im}(F(010|222)), \tag{C13}$$

$$Q_{zzz} = \frac{1}{\alpha}\left[\sqrt{\frac{2}{3}}\text{Im}(F(010|220)) - \frac{1}{\sqrt{3}}\text{Im}(F(010|200))\right]. \tag{C14}$$

When electric and magnetic fields are crossed at an arbitrary angle, the individual elements of the flux tensor are given by

$$Q_{xxy} = \frac{1}{\sqrt{2}\alpha}[\text{Re}(F(011|222)) - \text{Re}(F(01-1|222))], \tag{C15}$$

$$Q_{yxx} = \frac{\sqrt{2}}{\alpha}\left[\frac{1}{\sqrt{3}}\text{Re}(F(011|200)) + \frac{1}{\sqrt{6}}\text{Re}(F(011|220))\right] + \frac{1}{\sqrt{2}\alpha}[-\text{Re}(F(011|222))-\text{Re}(F(01-1|222))], \tag{C16}$$

$$Q_{yyy} = \frac{\sqrt{2}}{\alpha}\left[\frac{1}{\sqrt{3}}\text{Re}(F(011|200)) + \frac{1}{\sqrt{6}}\text{Re}(F(011|220))\right] + \frac{1}{\sqrt{2}\alpha}[\text{Re}(F(011|222)) + \text{Re}(F(01-1|222))], \tag{C17}$$

$$Q_{yzz} = \frac{\sqrt{2}}{\alpha}\left[\frac{1}{\sqrt{3}}\text{Re}(F(011|200)) - \sqrt{\frac{2}{3}}\text{Re}(F(011|220))\right], \tag{C18}$$

$$Q_{zxy} = -\frac{1}{\alpha}\text{Re}(F(010|222)), \tag{C19}$$

$$Q_{zyz} = \frac{1}{\alpha}\text{Re}(F(010|221)), \tag{C20}$$

$$Q_{xyz} = \frac{1}{\sqrt{2}\alpha}[\text{Re}(F(01-1|221))-\text{Re}(F(011|221))], \tag{C21}$$

$$Q_{yxz} = \frac{1}{\sqrt{2}\alpha}[\text{Re}(F(011|221))+\text{Re}(F(01-1|221))]. \tag{C22}$$

The elements of the third-order transport coefficients that are independent in a crossed field configuration, are also independent when the electric and magnetic fields cross at an arbitrary angle. Thus, the corresponding expressions in the Boltzmann equation analysis are identical.

In what follows, we present the explicit expressions for the flux components of the third-order transport coefficient tensor that might be identified and computed in our Monte Carlo simulations.

For parallel electric and magnetic fields, the explicit expressions of the flux longitudinal and flux transverse third-order transport coefficients are given by Eqs. (48) and (49), respectively. We are not able to isolate the additional elements of the tensor in the Monte Carlo method used in the present work. As already discussed in this Appendix, the coefficients Q_{xxz}, Q_{xyz}, Q_{zxx}, and $Q_L \equiv Q_{zzz}$ could be identified and computed using Boltzmann equation solutions.

For perpendicular electric and magnetic fields, we are able to identify six components of the third-order transport coefficient tensor in our Monte Carlo simulations. The tensor components are

$$Q_L \equiv Q_{zzz}, \quad Q_{E \times B} \equiv Q_{xxx} \tag{C23}$$

and

$$Q_{\pi(xxz)} \equiv \tfrac{1}{3}(Q_{xxz} + Q_{xzx} + Q_{zxx}), \tag{C24}$$

$$Q_{\pi(yyx)} \equiv \tfrac{1}{3}(Q_{yyx} + Q_{yxy} + Q_{xyy}) \tag{C25}$$

$$Q_{\pi(yyz)} \equiv \tfrac{1}{3}(Q_{yyz} + Q_{yzy} + Q_{zyy}), \tag{C26}$$

$$Q_{\pi(zzx)} \equiv \tfrac{1}{3}(Q_{zzx} + Q_{zxz} + Q_{xzz}), \tag{C27}$$

where the cross product $\boldsymbol{E} \times \boldsymbol{B}$ defines the x axis while $\pi(abc)$ denotes all possible permutations of (a, b, c). The explicit expressions of the flux tensor components are given by

$$Q_{zzz} = \tfrac{1}{6}(3\langle z^2 c_z \rangle - 3\langle c_z \rangle \langle z^2 \rangle - 6\langle z \rangle \langle z c_z \rangle + 6\langle z \rangle \langle z \rangle \langle c_z \rangle), \tag{C28}$$

$$Q_{xxx} = \tfrac{1}{6}(3\langle x^2 c_x \rangle - 3\langle c_x \rangle \langle x^2 \rangle - 6\langle x \rangle \langle x c_x \rangle + 6\langle x \rangle \langle x \rangle \langle c_x \rangle), \tag{C29}$$

$$Q_{xzz} = \tfrac{1}{6}(\langle z^2 c_x \rangle + 2\langle zx c_z \rangle - 2\langle c_z \rangle \langle zx \rangle - \langle c_x \rangle \langle z^2 \rangle - 2\langle z \rangle \langle x c_z \rangle - 2\langle z \rangle \langle z c_x \rangle - 2\langle x \rangle \langle z c_z \rangle + 2\langle c_x \rangle \langle z \rangle \langle z \rangle + 4\langle x \rangle \langle z \rangle \langle c_z \rangle), \tag{C30}$$

$$Q_{zxx} = \tfrac{1}{6}(\langle x^2 c_z \rangle + 2\langle xz c_x \rangle - 2\langle c_x \rangle \langle xz \rangle - \langle c_z \rangle \langle x^2 \rangle - 2\langle x \rangle \langle z c_x \rangle - 2\langle x \rangle \langle x c_z \rangle - 2\langle z \rangle \langle x c_x \rangle + 2\langle c_z \rangle \langle x \rangle \langle x \rangle + 4\langle z \rangle \langle x \rangle \langle c_x \rangle), \tag{C31}$$

$$Q_{zyy} = \tfrac{1}{6}(\langle y^2 c_z \rangle + 2\langle yz c_y \rangle - \langle c_z \rangle \langle y^2 \rangle - 2\langle z \rangle \langle y c_y \rangle), \tag{C32}$$

$$Q_{xyy} = \tfrac{1}{6}(\langle y^2 c_x \rangle + 2\langle yx c_y \rangle - \langle c_x \rangle \langle y^2 \rangle - 2\langle x \rangle \langle y c_y \rangle). \tag{C33}$$

For the most general case when electric and magnetic fields are crossed at an arbitrary angle, we are able to identify 10 components of the third-order transport coefficient tensor in our Monte Carlo simulation code. They include six components already defined for perpendicular electric and magnetic fields and four additional coefficients, including

$$Q_{E \times (E \times B)} \equiv Q_{yyy}, \tag{C34}$$

where the cross product $\boldsymbol{E} \times (\boldsymbol{E} \times \boldsymbol{B})$ defines the y axis, and

$$Q_{\pi(xxy)} \equiv \tfrac{1}{3}(Q_{xxy} + Q_{xyx} + Q_{yxx}), \tag{C35}$$

$$Q_{\pi(zzy)} \equiv \tfrac{1}{3}(Q_{zzy} + Q_{zyz} + Q_{yzz}), \tag{C36}$$

$$Q_{\pi(xyz)} \equiv \tfrac{1}{6}(Q_{xyz} + Q_{yzx} + Q_{zxy} + Q_{xzy} + Q_{yxz} + Q_{zyx}). \tag{C37}$$

The remaining explicit expressions for the flux components of the third-order transport coefficient tensor are given by

$$Q_{yyy} = \tfrac{1}{6}(3\langle y^2 c_y \rangle - 3\langle c_y \rangle \langle y^2 \rangle - 6\langle y \rangle \langle y c_y \rangle + 6\langle y \rangle \langle y \rangle \langle c_y \rangle), \tag{C38}$$

$$Q_{xyz} = \tfrac{1}{6}(\langle yz c_x \rangle + \langle xz c_y \rangle + \langle xy c_z \rangle - \langle c_x \rangle \langle yz \rangle - \langle x \rangle \langle z c_y \rangle - \langle x \rangle \langle y c_z \rangle - \langle c_y \rangle \langle xz \rangle - \langle y \rangle \langle z c_x \rangle - \langle y \rangle \langle x c_z \rangle - \langle c_z \rangle \langle xy \rangle$$
$$- \langle z \rangle \langle y c_x \rangle - \langle z \rangle \langle x c_y \rangle + 2\langle c_x \rangle \langle y \rangle \langle z \rangle + 2\langle c_y \rangle \langle x \rangle \langle z \rangle + 2\langle c_z \rangle \langle y \rangle \langle x \rangle), \tag{C39}$$

$$Q_{yxx} = \tfrac{1}{6}(\langle x^2 c_y \rangle + 2\langle yx c_x \rangle - 2\langle c_x \rangle \langle yx \rangle - \langle c_y \rangle \langle x^2 \rangle - 2\langle x \rangle \langle y c_x \rangle - 2\langle x \rangle \langle x c_y \rangle - 2\langle y \rangle \langle x c_x \rangle + 2\langle c_y \rangle \langle x \rangle \langle x \rangle + 4\langle y \rangle \langle x \rangle \langle c_x \rangle), \tag{C40}$$

$$Q_{yzz} = \tfrac{1}{6}(\langle z^2 c_y \rangle + 2\langle yz c_z \rangle - 2\langle c_z \rangle \langle yz \rangle - \langle c_y \rangle \langle z^2 \rangle - 2\langle z \rangle \langle y c_z \rangle - 2\langle z \rangle \langle z c_y \rangle - 2\langle y \rangle \langle z c_z \rangle + 2\langle c_y \rangle \langle z \rangle \langle z \rangle + 4\langle y \rangle \langle z \rangle \langle c_z \rangle), \tag{C41}$$

$$Q_{zyy} = \tfrac{1}{6}(\langle y^2 c_z \rangle + 2\langle yz c_y \rangle - 2\langle c_y \rangle \langle yz \rangle - \langle c_z \rangle \langle y^2 \rangle - 2\langle y \rangle \langle z c_y \rangle - 2\langle y \rangle \langle y c_z \rangle - 2\langle z \rangle \langle y c_y \rangle + 2\langle c_z \rangle \langle y \rangle \langle y \rangle + 4\langle z \rangle \langle y \rangle \langle c_y \rangle), \tag{C42}$$

$$Q_{xyy} = \tfrac{1}{6}(\langle y^2 c_x \rangle + 2\langle yx c_y \rangle - 2\langle c_y \rangle \langle yx \rangle - \langle c_x \rangle \langle y^2 \rangle - 2\langle y \rangle \langle x c_y \rangle - 2\langle y \rangle \langle y c_x \rangle - 2\langle x \rangle \langle y c_y \rangle + 2\langle c_x \rangle \langle y \rangle \langle y \rangle + 4\langle x \rangle \langle y \rangle \langle c_y \rangle). \tag{C43}$$

[1] L. G. H. Huxley and R. W. Crompton, *The Diffusion and Drift of Electrons in Gases* (Wiley, London, 1974).

[2] E. A. Mason and E. W. McDaniel, *Transport Properties of Ions in Gases* (Wiley, New York, 1988).

[3] R. W. Crompton, Adv. At. Mol. Opt. Phys. **32**, 97 (1994).

[4] Z. Lj. Petrović, M. Šuvakov, Ž. Nikitović, S. Dujko, O. Šašić, J. Jovanović, G. Malović, and V. Stojanović, Plasma Sources Sci. Technol. **16**, S1 (2007).

[5] R. D. White, D. Cocks, G. Boyle, M. Casey, N. Garland, D. Konovalov, B. Philippa, P. Stokes, J. de Urquijo, O. Gonzales-Magana, R. P. McEachran, S. J. Buckman, M. J. Brunger, G. Garcia, S. Dujko, and Z. Lj. Petrović, Plasma Sources Sci. Technol. **27**, 053001 (2018).

[6] T. Makabe and Z. Lj. Petrović, *Plasma Electronics: Applications in Microelectronic Device Fabrication* (CRC Press, New York, 2014).

[7] M. A. Lieberman and A. J. Lichtenberg, *Principles of Plasma Discharges and Materials Processing* (Wiley Interscience, Hoboken, NJ, 2005).

[8] L. L. Alves, A. Bogaerts, V. Guerra, and M. M. Turner, Plasma Sources Sci. Technol. **27**, 023002 (2018).

[9] I. Adamovich, S. D. Baalrud, A. Bogaerts, P. J. Bruggeman, M. Cappelli, V. Colombo, U. Czarnetzki, U. Ebert, J. G. Eden, P. Favia, D. B. Graves, S. Hamaguchi, G. Hieftje, M. Hori, I. D. Kaganovich, U. Kortshagen, M. J. Kushner, N. J. Mason, S. Mazouffre, S. Mededovic Thagard, H. R. Metelmann, A. Mizuno, E. Moreau, A. B. Murphy, B. A. Niemira, G. S. Oehrlein, Z. Lj. Petrovic, L. C. Pitchford, Y. K. Pu, S. Rauf, O. Sakai, S. Samukawa, S. Starikovskaia, J. Tennyson, K. Terashima, M. M. Turner, M. C. M. Van De Sanden, and A. Vardelle, J. Phys. D: Appl. Phys. **50**, 323001 (2017).

[10] L. Rolandi, W. Riegler, and W. Blum, *Particle Detection with Drift Chambers* (Springer, Berlin, 2008).

[11] D. Bošnjaković, Z. Lj. Petrović, R. D. White, and S. Dujko, J. Phys. D: Appl. Phys. **47**, 435203 (2014).

[12] D. Xiao, *Gas Discharge and Gas Insulation* (Springer, Heidelberg, 2016).

[13] M. Charlton and J. W. Humberston, *Positron Physics* (Cambridge University Press, Cambridge, 2001).

[14] Z. Lj. Petrović, A. Banković, S. Dujko, S. Marjanović, G. Malović, J. P. Sullivan, and S. Buckman, in *Eighth International Conference on Atomic and Molecular Data and Their Applications: ICAMDATA-2012*, edited by J. D. Gillaspy, W. L. Wiese, and Y. A. Podpaly, AIP Conf. Proc. No. 1545 (AIP, New York, 2013).

[15] L. C. Pitchford *et al.*, Plasma Process. Polym. **14**, 1600098 (2016).

[16] Z. Lj. Petrović, S. Dujko, D. Marić, G. Malović, Ž. Nikitović, O. Šašić, J. Jovanović, V. Stojanović, and M. Radmilović-Rađenović, J. Phys. D: Appl. Phys. **42**, 194002 (2009).

[17] R. D. White, S. Dujko, R. E. Robson, Z. Lj. Petrović, and R. P. McEachran, Plasma Sources Sci. Techol. **19**, 034001 (2010).

[18] B. M. Penetrante and J. N. Bardsley, in *Non-equilibrium Effects in Ion and Electron Transport*, edited by J. W. Gallagher, D. F. Hudson, E. E. Kunhardt, and R. J. Van Brunt (Plenum, New York, 1990), p. 49.

[19] S. B. Vrhovac, Z. Lj. Petrović, L. A. Viehland, and T. S. Santhanam, J. Chem. Phys. **110**, 2423 (1999).

[20] J. H. Schummers, G. M. Thomson, D. R. James, I. R. Gatland, and E. W. McDaniel, Phys. Rev. A **7**, 683 (1973).

[21] S. R. Hunter, Ph.D. thesis, Flinders University, Adelaide, Australia (1977).

[22] H. A. Blevin, J. Fletcher, and S. R. Hunter, J. Phys. D: Appl. Phys. **9**, 471 (1976).

[23] H. A. Blevin, J. Fletcher, and S. R. Hunter, Aust. J. Phys. **31**, 299 (1978).

[24] C. A. Denman and L. A. Schlie, in *Non-equilibrium Effects in Ion and Electron Transport*, Proceedings of the 6th International Swarm Seminar, Glen Cove, NY, edited by J. W. Gallagher *et al.* (Springer, New York, 1989), p. 359.

[25] J. H. Whealton and E. A. Mason, Ann. Phys. **84**, 8 (1974).

[26] R. Robson, Aust. J. Phys. **28**, 523 (1975).

[27] P. H. Larsen, H. R. Skullerud, T. H. Lovaas, and T. Stefansson, J. Phys. B: At. Mol. Opt. Phys. **21**, 2519 (1988).

[28] K. Kondo and H. Tagashira, J. Phys. D: Appl. Phys. **23**, 1175 (1990).

[29] A. D. Koutselos, J. Chem. Phys. **104**, 8442 (1996).

[30] A. D. Koutselos, J. Chem. Phys. **106**, 7117 (1997).

[31] A. D. Koutselos, Chem. Phys. **270**, 165 (2001).

[32] A. D. Koutselos, Chem. Phys. **315**, 193 (2005).

[33] R. E. Robson, J. Chem. Phys. **85**, 4486 (1986).

[34] S. B. Vrhovac and Z. Lj. Petrović, Phys. Rev. E **53**, 4012 (1996).

[35] S. Kawaguchi, K. Takahashi, and K. Satoh, Plasma Sources Sci. Technol. **27**, 085006 (2018).

[36] S. Kawaguchi, K. Takahashi, and K. Satoh, in *Proceedings of the 22nd International Conference on Gas Discharges and Their Applications, Novi Sad, Serbia*, edited by Z. Lj. Petrović, N. Puač, S. Dujko, and N. Škoro (Serbian Academy of Sciences and Arts, Belgrade, 2018), p. 531.

[37] S. Dujko, R. D. White, and Z. Lj. Petrović, J. Phys. D: Appl. Phys. **41**, 245205 (2008).

[38] Z. Lj. Petrović, I. Simonović, S. Marjanović, D. Bošnjaković, D. Marić, G. Malović, and S. Dujko, Plasma Phys. Control. Fusion **59**, 014026 (2017).

[39] P. W. Stokes, I. Simonović, B. Philippa, D. Cocks, S. Dujko, and R. D. White, Sci. Rep. **8**, 2226 (2018).

[40] C. Li, W. J. M. Brok, U. Ebert, and J. J. A. M. van der Mullen, J. Appl. Phys. **101**, 123305 (2007)

[41] A. H. Markosyan, S. Dujko, and U. Ebert, J. Phys. D: Appl. Phys. **46**, 475203 (2013).

[42] Z. M. Raspopović, S. Dujko, R. D. White, and Z. Lj. Petrović, IEEE Trans. Plasma. Sci. **39**, 2566 (2011).

[43] S. Dujko, Z. M. Raspopović, R. D. White, T. Makabe, and Z. Lj. Petrović, Eur. Phys. J. D **68**, 166 (2014).

[44] M. Šuvakov, Z. Ristivojević, Z. Lj. Petrović, S. Dujko, Z. M. Raspopović, N. A. Dyatko, and A. P. Napartovich, IEEE Trans. Plasma Sci. **33**, 532 (2005).

[45] J. Mirić, D. Bošnjaković, I. Simonović, Z. Lj. Petrović, and S. Dujko, Plasma Sources Sci. Technol. **25**, 065010 (2006).

[46] M. Šuvakov, Z. Lj. Petrović, J. P. Marler, S. J. Buckman, R. E. Robson, and G. Malović, New J. Phys. **10**, 053034 (2008).

[47] A. Banković, S. Dujko, R. D. White, S. J. Buckman, and Z. Lj. Petrović, Nucl. Instrum. Meth. Phys. Res. B **279**, 92 (2011).

[48] R. T. Sibatov and V. V. Uchaikin, Semiconductors **41**, 335 (2007).

[49] M. Schubert, E. Preis, J. C. Blakesley, P. Pingel, U. Scherf, and D. Neher, Phys. Rev. B **87**, 024203 (2013).

[50] H. Krüsemann, A. Godec, and R. Metzler, Phys. Rev. E **89**, 040101(R) (2014).

[51] H. Krüsemann, R. Schwarzl, and R. Metzler, Transp. Porous Media **115**, 327 (2016).

[52] A. Mauracher, M. Daxner, J. Postler, S. E. Huber, S. Denifl, P. Scheier, and J. P. Toennies, J. Phys. Chem. Lett. **5**, 2444 (2014).

[53] A. F. Borghesani and M. Santini, Phys. Rev. E **65**, 056403 (2002).

[54] Y. Sakai, W. F. Schmidt, and A. Khrapak, Chem. Phys. **164**, 139 (1992).

[55] S. V. Stepanov, V. M. Byakov, D. S. Zvezhinskiy, G. Duplâtre, R. R. Nurmukhametov, and P. S. Stepanov, Adv. Phys. Chem. **2012**, 431962 (2012).

[56] S. V. Stepanov, V. M. Byakov, B. N. Ganguly, D. Gangopadhyay, T. Mukherjee, and B. Dutta-Roy, Physica B: Condens. Matter **322**, 68 (2002).

[57] K. Norregaard, R. Metzler, C. M. Ritter, K. Berg-Sørensen, and L. B. Oddershede, Chem. Rev. **117**, 4342 (2017).

[58] M. Schwarzl, A. Godec, and R. Metzler, Sci. Rep. **7**, 3878 (2017).

[59] F. Höfling and T. Franosch, Rep. Prog. Phys. **76**, 046602 (2013).

[60] M. Magdziarz, A. Weron, K. Burnecki, and J. Klafter, Phys. Rev. Lett. **103**, 180602 (2009).

[61] K. F. Ness and R. E. Robson, Phys. Rev. A **34**, 2185 (1986)

[62] R. Robson, R. White, and M. Hildebrandt, *Fundamentals of Charged Particle Transport in Gases and Condensed Matter* (CRC Press, Boca Raton, FL, 2018).

[63] K. Kumar, H. R. Skullerud, and R. E. Robson, Aust. J. Phys. **33**, 343 (1980).

[64] S. Dujko, R. D. White, Z. M. Raspopović, and Z. Lj. Petrović, Nucl. Instrum. Meth. Phys. Res. B **279**, 84 (2012).

[65] M. Damnjanović and I. Milošević, J. Phys. A: Math. Gen. **28**, 1669 (1995).

[66] R. D. White, R. E. Robson, S. Dujko, P. Nicoletopoulos, and B. Li, J. Phys. D: Appl. Phys. **42**, 194001 (2009).

[67] S. Dujko, R. D. White, Z. Lj. Petrović, and R. E. Robson, Phys. Rev. E **81**, 046403 (2010).

[68] S. Dujko, R. D. White, Z. Lj. Petrović, and R. E. Robson, Plasma Sources Sci. Technol. **20**, 024013 (2011).

[69] R. E. Robson and K. F. Ness, Phys. Rev. A **33**, 2068 (1986).

[70] R. D. White, K. F. Ness, R. E. Robson, and B. Li, Phys. Rev. E **60**, 2231 (1999).

[71] Z. M. Raspopović, S. Sakadžić, S. Bzenić, and Z. Lj. Petrović, IEEE Trans. Plasma Sci. **27**, 1241 (1999).

[72] Z. Lj. Petrović, Z. M. Raspopović, S. Dujko, and T. Makabe, Appl. Surf. Sci. **192**, 1 (2002).

[73] S. Dujko, Z. M. Raspopović, and Z. Lj. Petrović, J. Phys. D: Appl. Phys. **38**, 2952 (2005).

[74] I. Simonović, Z. Lj. Petrović, and S. Dujko, in *Proceedings of the 27th Symposium on Physics of Ionized Gases—SPIG 2014, Belgrade, Serbia*, edited by D. Marić, A. R. Milosavljević, and Z. Mijatović, Contributed Papers and Abstracts of Invited Lectures, Topical Invited Lectures. Progress Reports and Workshop Lectures (Institute of Physics, Belgrade & Klett izdavacka kuca d.o.o., Belgrade, 2014), pp. 138–141.

[75] I. Simonović, Z. Lj. Petrović, R. D. White, D. Bošnjaković, and S. Dujko, in *Proceedings of the 22nd International Conference on Gas Discharges and Their Applications—GD 2018, Novi Sad, Serbia*, edited by Z. Lj. Petrović, N. Puač, S. Dujko, and N. Škoro (Serbian Academy of Sciences and Arts, Belgrade, 2018), pp. 551–554.

[76] I. Simonović, Z. Lj. Petrović, R. D. White, D. Bošnjaković, and S. Dujko, in *Proceedings of the 29th Symposium on Physics of Ionized Gases—SPIG 2018, Belgrade, Serbia*, edited by G. Poparić, B. Obradović, D. Borka, and M. Rajković, Contributed Papers and Abstracts of Invited Lectures, Topical Invited Lectures. Progress Reports and Workshop Lectures, (Vinča Institute of Nuclear Sciences, University of Belgrade, Belgrade, 2018), pp. 67–70.

[77] M. Hayashi (private commutation, 2000).

[78] R. D. White, R. E. Robson, P. Nicoletopoulos, and S. Dujko, Eur. Phys. J. D **66**, 117 (2012).

[79] L. Boltzmann, Wein. Ber. **66**, 275 (1872).

[80] C. S. Wang-Chang, G. E. Uhlenbeck, and J. DeBoer, in *Studies in Statistical Mechanics*, edited by J. DeBoer and G. E. Uhlenbeck (Wiley, New York, 1964), Vol. 2, p. 241.

[81] Z. Ristivojević and Z. Lj. Petrović, Plasma Sources Sci. Technol. **21**, 035001 (2012).

[82] K. F. Ness, J. Phys. D: Appl. Phys. **27**, 1848 (1994).

[83] R. D. White, M. J. Brennan, and K. F. Ness, J. Phys. D: Appl. Phys. **30**, 810 (1997).

[84] R. D. White, R. E. Robson, and K. F. Ness, Comput. Phys. Commun. **142**, 349 (2001).

[85] I. D. Reid, Aust. J. Phys. **32**, 231 (1979).

[86] S. Marjanović, A. Banković, D. Cassidy, B. Cooper, A. Deller, S. Dujko, and Z. Lj. Petrović, J. Phys. B: At. Mol. Opt. Phys. **49**, 215001 (2016).

[87] S. Marjanović and Z. Lj. Petrović, Plasma Sources Sci. Technol. **26**, 024003 (2017).

[88] S. Marjanović, M. Šuvakov, A. Banković, M. Savić, G. Malović, S. J. Buckman, and Z. Lj. Petrović, IEEE Trans. Plasma Sci. **39**, 2614 (2011).

[89] Z. Lj. Petrović, S. Marjanović, S. Dujko, A. Banković, G. Malović, S. Buckman, G. Garcia, R. White, and M. Brunger, Appl. Radiat. Isotop. **83**, 148 (2014).

[90] M. R. Natisin, J. R. Danielson, and C. M. Surko, J. Phys. B: At. Mol. Opt. Phys. **47**, 225209 (2014).

[91] L. M. Blinov, *Structure and Properties of Liquid Crystals* (Springer, New York, 2011).

[92] W. K. Tung, *Group Theory in Physics* (World Scientific, Singapore, 1984).

[93] A. O. Barut and R. Raczka, *Theory of Group Representations and Applications* (Polish Scientific Publishers, Warsaw, 1980).

[94] F. P. Temme and B. C. Sanctuary, J. Magn. Reson. **69**, 1 (1986).

[95] R. E. Robson, Phys. Rev. A **13**, 1536 (1976).

[96] R. E. Robson, Phys. Rev. E **61**, 848 (2000).